

Calculation of UVI for Smartphone Apps

Richard McKenzie, NIWA Lauder.

What is the UVI?

The WHO and WMO recommend that UV information is provided to the public in terms of the UV Index (UVI).¹ The UVI is a measure of the strength of sun-burning radiation. It ranges from zero when it dark, to peak global values that can exceed 25 in the tropical Andes.² For fair-skinned populations at temperate latitudes, UVI values of 11 or more are considered “extreme”. For those UVI values, damage to the most sensitive skin types can occur in less than 15 minutes.³ The UVI was originally used in Canada, where the scale was chosen so that the maximum summer value reached 10 in that country.

At mid-latitudes, there is a large seasonal variability in peak noon values, ranging from about 1 at the winter solstice, to about 10 at the summer solstice, as illustrated below.

The UVI is found by weighting the spectrum of sunlight by the erythemal action spectrum,⁴ which is a measure of the relative damage to skin as a function of wavelength (see Figure 1, left panel). The resulting function is the erythemally weighted UV spectral irradiance (in units of $\text{Wm}^{-2}\text{nm}^{-1}$). The integral over wavelength (i.e., the area under the curve), is the “erythemally weighted” UV (sometimes called the erythemal UV, UV_{ery} , in units of Wm^{-2}). This small number is then multiplied by a scale factor $40/(\text{Wm}^{-2})$ to give the UVI (see Figure 1, right panel), which was originally used in Canada, where the maximum summer value reached 10. For example, when $\text{UV}_{\text{ery}} = 0.25 \text{ Wm}^{-2}$, the corresponding UVI is 10 (unitless).

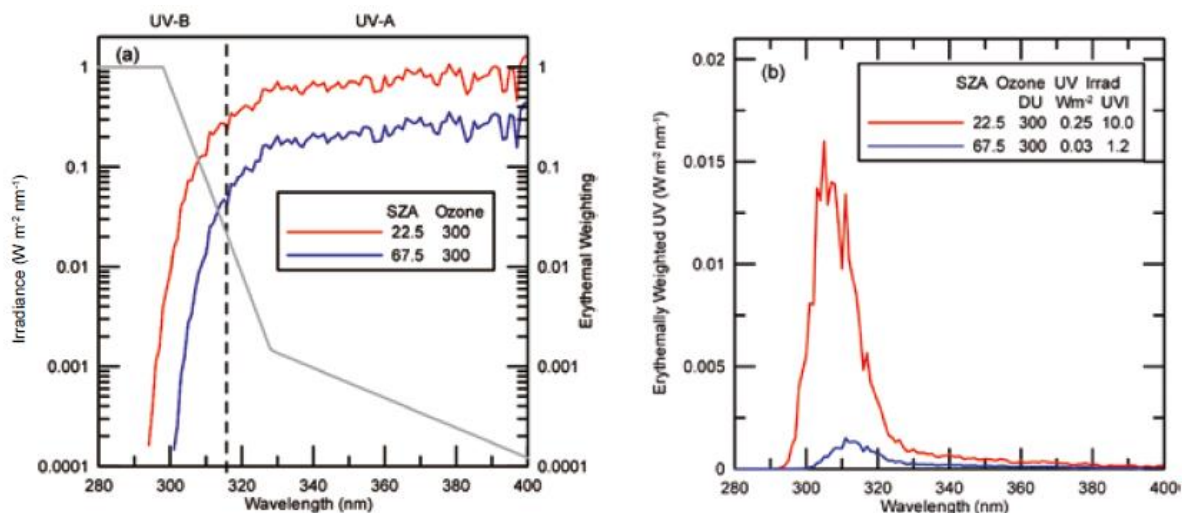


Figure 1. Measurements at the summer and winter solstices at Lauder New Zealand (45°S) to illustrate the definition and variability of erythemally-weighted UV and the UV Index (UVI).

Apps that calculate UVI must be able to store the necessary invariant fields, such as elevation, and to quickly upload the variable fields, such as the total atmospheric ozone amounts. They must then make use of GPS location co-ordinates, and the date/time to calculate the solar zenith angle (SZA). A reference clear sky UV, which is a function of SZA and ozone, can then be calculated.

Calculation of Clear Sky UVI

The GlobalUV app will eventually supersede the uv2Day app, which applies only in the New Zealand, Australia, and Pacific region, where aerosol extinctions are small. In this app, forecast UVI values can be provided at any phone location. UVI can also be calculated at any of about 350 pre-loaded sites for which latitude, altitude, and longitude are specified. Other sites can be added by the users by specifying their co-ordinates as above

In apps of this sort, the clear sky UVI at sea level is first calculated from the solar zenith angle (SZA) and from ozone forecast fields provided by NOAA. The first step is to provide a pre-calculated lookup table of UVI values as a function of these variables (at 5 degree steps in SZA) and 5 UD steps in ozone respectively, calculated for a sun-earth separation of 1 AU, and for a surface albedo of 0.05 (i.e., 5% reflection at wavelengths around 305 nm). This lookup table is named: Lookup_step5_alt0.0km.dat. The dependence of UVI on ozone and SZA is illustrated in Figure 2.

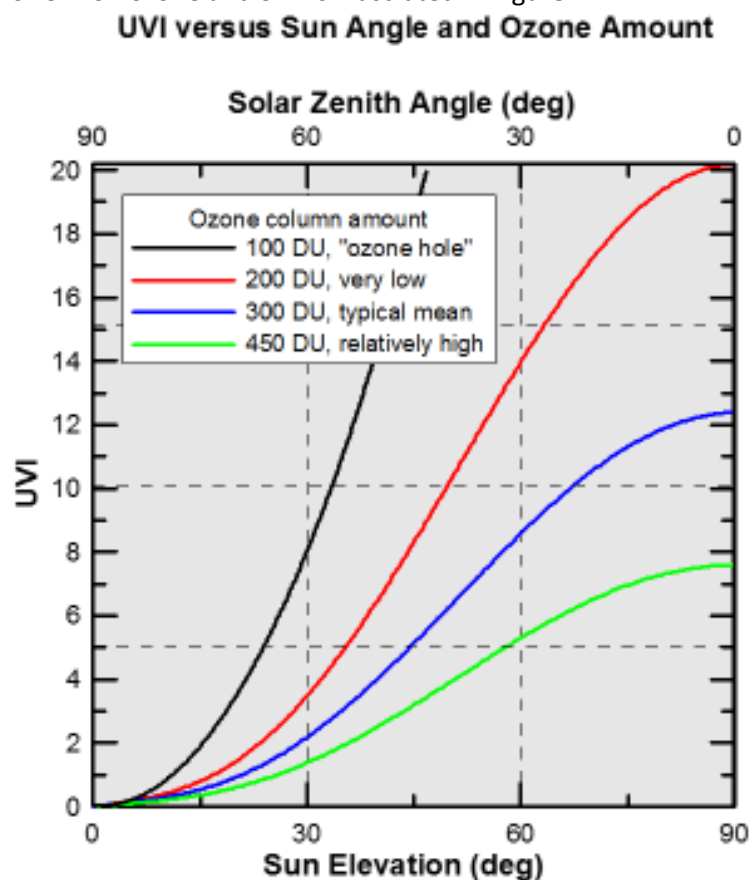


Figure 2. UVI as a function of solar elevation (and SZA = 90 – solar elevation) for several ozone amounts.

UVI results are returned by linear interpolation of that table, using the SZA calculated from GPS data, and interpolation of gridded ozone forecast data.

A description of the ozone forecast files, and their locations, and extraction of the most appropriate file is discussed elsewhere. See file:

1. Accessing Ozone forecast files.pdf
2. Algorithm for Selection of Best Ozone File.pdf

These files can be made available as appendices to this document.

Perturbations to Clear Sky UVI Calculation

After calculating the clear sky UV Index for 1AU at sea level (UVI_0 (ozone, SZA)), corrections factors are applied to take account of:

- Seasonal changes in Sun-Earth separation, $f_{S-E}(doy)$
- Variations in altitude, $f_{Alt}(alt)$
- Variation in aerosol optical depth, $f_{Aer}(aod)$
- Variations in surface albedo, $f_{Alb}(snow, alt)$
- Variations in cloud cover, f_{Cloud}

Finally,

$UVI = UVI_0 * f_{S-E} * f_{Alt} * f_{Aer} * f_{Alb} * f_{Cloud}$, where, as discussed in detail in the following section,

$$f_{S-E} = 1 + [0.032 * \cos(2\pi * DoY/365)]$$

$f_{Alt} = 1 + [0.053 * Alt]$ (when changes due to changes in pressure and changes in overhead ozone column are combined, the increases with altitude are nearly linear)

$$f_{Aer} = [\exp(-0.339 * AOD_{368nm})]$$

$$f_{Alb} = 1 + [0.4 * Alb * \exp(-Alt/7.65)], \text{ (for alt in km)}$$

$$f_{Cloud} = | 1.0 \text{ (for sun not obscured, default, else} \\ | (\exp(-Alt/7.65))^{0.4} * (1 + 0.15 * Alb) - 0.6 * (1 - AOD_{368nm}) * (\cos(\pi * sza/180))^{0.9},$$

For sun-obscured, yielding approximately 0.5 for high sun

Alternatively, f_{cloud} can be input directly from a cloud forecast

Procedures to quantitatively deal with these effects are described in the following section.

Similar procedures can be applied to other UV apps, although the last three correction factors above depend on the spectral weighting factors. For example, UVA has a smaller dependence than UVI on altitude, aerosols, and surface albedo.

An alternative procedure, where a lookup table of UVI value as a function of pre-calculated as functions of 5 independent variables (SZA, ozone, altitude, aerosol optical depth, surface albedo), is also possible. If this more complex (and large) 5-dimensional lookup table is used, then the only perturbation required in the Sun-Earth correction factor above. See the appendix for a sample showing the format of this lookup file.

Sun-Earth Factor

The orbit of Earth about the Sun is elliptical, rather than circular. Closest approach (perihelion) near 2 January, and it is most distant near 2 July (aphelion). The mean Sun-Earth separation (1 AU) occurs near 2 April and 2 September, and the separation varies by approximately 1.7% between perihelion and aphelion. The effect on radiation arriving at Earth's surface is calculated from the inverse square law, so the correction factor (f_{S-E}) is given by

$$f_{S-E} = 1 + [0.032 * \cos(2\pi * doy/365)], \text{ where } doy = \text{day of year.}$$

Locations and Elevations

The 350 sites included the GlobalUV app are shown in Figure 3. The sites are a composite of all of the TEMIS sites, the uv2Day sites, and several extra sites selected to complete coverage in data-sparse areas such as Africa, South America, Australia, and the Pacific Islands.

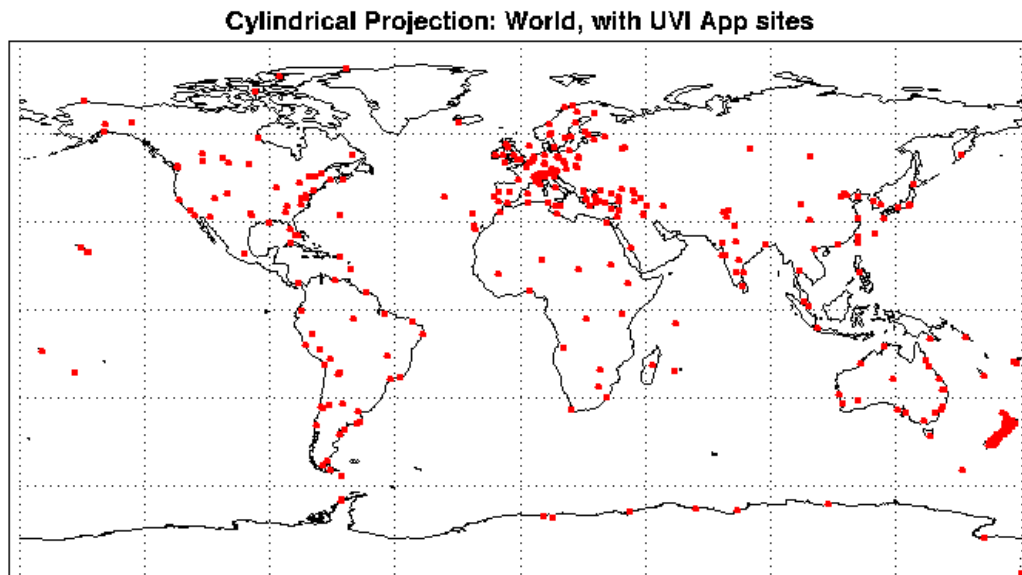


Figure 3. Red symbols show the locations of the 350 specified sites (plot generated by IDL code named Map UVI App.pro).

Altitude data are input at 0.5 degree resolution, which corresponds to a pixel size of about 50 km at the equator, with the East=West extent decreasing progressively at larger latitudes. The altitude data same can be used to estimate altitude effects, and seasonally varying albedo effects, using relationships between altitude and snow cover. Figure 4 shows these same sites plotted on this altitude grid.

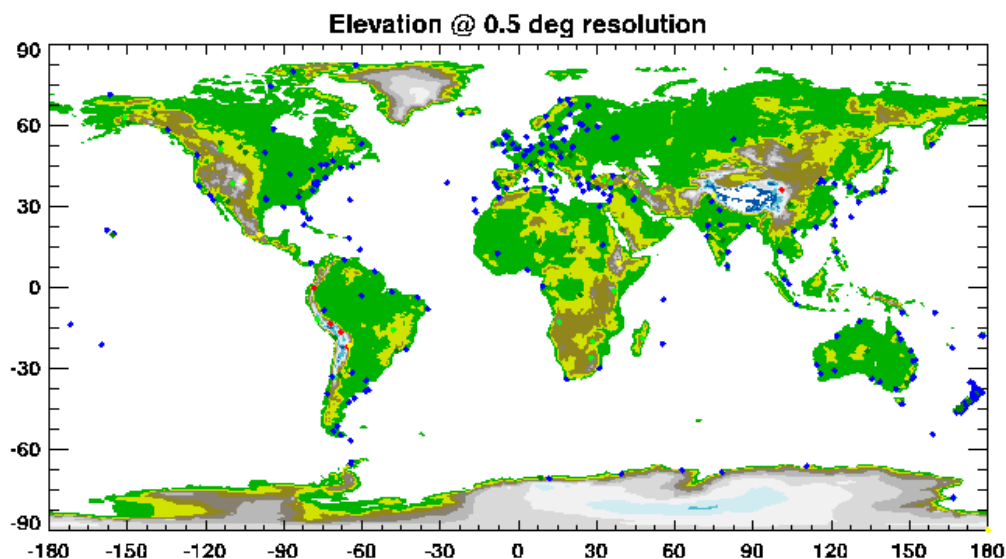


Figure 4. Blue symbols show the locations of the 350 specified sites overlaid on a colour-coded altitude grid that ranges from 0 to 4 km (plot generated by IDL code named Map UVI App.pro).

At localised mountain peaks, there can be significant differences between the actual altitude and its representation on a 0.5 degree grid, as shown in Figure 5. The largest errors are for Denali (i.e., Mt McKinley, Alaska), Canyonlands, and Mauna Loa Observatory.

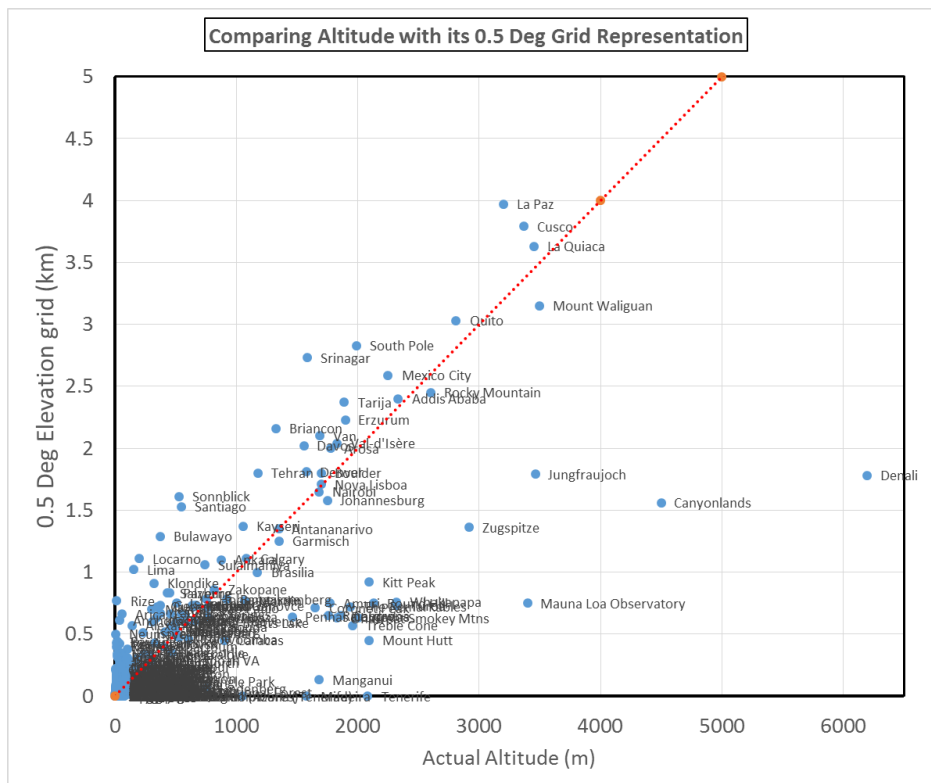


Figure 5. Scatterplot showing differences between the actual altitude (in m), and the gridded altitudes (in km) for the 350 specified sites.

Effect of Altitude on UVI

The tuv radiative transfer model was used to calculate the increase in clear-sky UVI as function of altitude. Results are shown in Table 1.

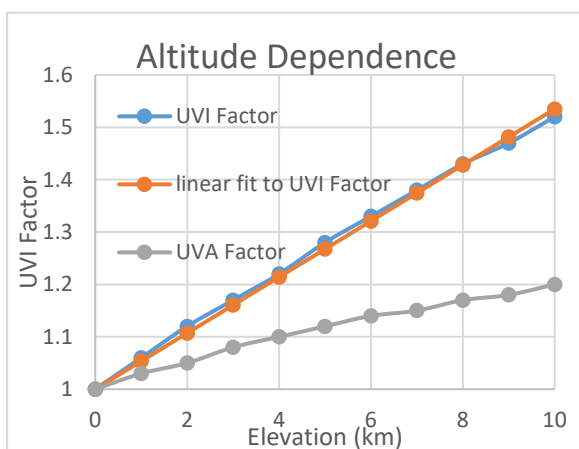
The calculation is for 1 Jan at 20S, for clear skies and a solar zenith angle (SZA) of 30 degrees. Absolute amounts would be about 10-15% greater for overhead sun. The rates of increase with altitude are similar for other locations and SZA.⁵ Thus, for aerosol free conditions, the altitudinal gradients are much smaller than stated in much of the literature. In clean air, UVI increases by 5.8% in the first km, and by smaller increments thereafter. In unpolluted conditions. At 10 km, UVI and UVB are about 50% more than at the surface in clean air, whereas UVA is about 20% higher.

In polluted locations, including most of the northern hemisphere, the surface irradiance will be further attenuated by at least 10% due mainly to aerosol extinctions in the lower troposphere (boundary layer). So the altitude gradient in the first one of two kilometres depends on how polluted the site is. However, above the boundary layer, the gradient would revert to those calculated below.

alt (km)	press (hPa)	ozone (DU)	uva	uvb	uvi	uva/ uvb	δ UVI/km (%)	Increase factor relative to surface value for clear skies and in clean air		
			(Wm-2)					UVI	UVA	UVB
0	1013	276	67.8	2.4	13.8	28.0				
1	899	275	69.7	2.6	14.6	27.3	5.8	1.06	1.03	1.05
2	795	273	71.4	2.7	15.4	26.5	5.5	1.12	1.05	1.11
3	702	272	73.0	2.8	16.2	25.9	5.2	1.17	1.08	1.16
4	617	271	74.5	2.9	16.9	25.4	4.3	1.22	1.10	1.21
5	541	269	75.9	3.1	17.7	24.8	4.7	1.28	1.12	1.26
6	473	268	77.1	3.2	18.4	24.4	4.0	1.33	1.14	1.31
7	412	266	78.3	3.3	19.1	23.8	3.8	1.38	1.15	1.36
8	357	265	79.3	3.4	19.7	23.5	3.1	1.43	1.17	1.40
9	309	264	80.2	3.5	20.3	1.0	3.0	1.47	1.18	1.46
10	266	262	81.1	3.6	21.0	22.7	3.4	1.52	1.20	1.47

Table 1. Calculated increases in clear-sky UVI (and other weightings) as a function of altitude

Radiative effects are caused by differences in pressure, rather than altitude itself, as the changes in altitude are negligible compared with the Sun-Earth separation. Atmospheric pressure reduces exponentially with altitude, and reaches $1/e^{\text{th}}$ of its surface value at an altitude of 7.65 km (called the “scale height” of the atmosphere). Thus, $p_h = p_0 * \exp(-\text{alt}/7.65)$. Because of ozone extinctions in the troposphere, there are slight departures from a simple pressure dependence for UVI (but not for UVA).



From Table 1 (see also figure alongside), we find that the altitude effect (including effects of smaller ozone column above), is near-linear, and is well approximated by:

$$f_{\text{Alt}} = 1 + [0.053 * \text{alt}]$$

The altitude effect on UVA is less than half of that for UVI.

Aerosols

Aerosol can have marked impact on UVI, especially in polluted regions, where the mean aerosol optical depth can approach unity,⁶ and peak values can approach 4⁷.

Even in relatively clean air, aerosol extinctions can have a significant effect on UVI. Data from the USDA's UV network indicate that they may be responsible for reductions in peak UVI of ~20% in rural USA compared with pristine locations such as Lauder New Zealand.⁸ This implies that the variable impact of aerosols on the UV Index should generally be considered. However, without near-real-time (NRT) availability of the UV optical properties this is hard to implement at present.

The European Space Agency (ESA) maintains the Tropospheric Emissions Monitoring Internet Service (TEMIS), which is a portal to provide satellite derived products such as the UV Index (see <http://www.temis.nl/uvradiation/nrt/uvindex.php>). These UVI products are part of the ECMWF's (European Centre for Medium Range Weather Forecasting) delivery service known as MACC/CAMS (the Monitoring of Atmospheric Composition and Climate/Copernicus Atmospheric Monitoring Service, see <https://www.gmes-atmosphere.eu/>). Currently, the products there do not include real time estimations of either clouds, or aerosols, as MACC/CAMS are not yet able to provide the NRT aerosol optical data needed. However, this might become possible soon, e.g., see: http://macc.copernicus-atmosphere.eu/d/services/gac/nrt/nrt_opticaldepth!03!Total!SE%20Asia!macc!od!enfo!nrt_opticaldepth!2015093000!2015093000_03/

In anticipation of such aerosol products, an aim of the 2002 report by Jordi Badosa (<http://bibliotheek.knmi.nl/knmipubWR/WR2002-07.pdf>)⁹ was to derive the UV effects from aerosol optical properties which are implicit in the TEMIS UV Index empirical algorithm (see p.29 of Allaart et al.,¹⁰). The current TEMIS UV Index aerosol correction climatology implicitly corresponds to an exponential fit (p 22,23; equations. 42, 43)⁹ with for the aerosol UV optical parameters globally constant values:

$$\begin{aligned} \text{UVI_TEMIS (AOD)} &= \text{UVI(AOD=0)} * \exp(-b * \text{AOD(368nm)}), \text{ where} \\ \text{AOD(368nm)} &= 0.3 \\ \mu_0 &= \cos(\text{SZA}) \\ b &= 0.30 + 0.74 * \mu_0 - 1.27 * \mu_0^2 + 0.54 * \mu_0^3 \\ &\text{and assuming SSA} = 0.9 \end{aligned}$$

The above equation assumes a single scattering albedo (SSA) of 0.9. Equation 44⁹ provides an expression to include variations in SSA (if known):

$$b(\text{SSA}) = b(0.9) * [1.0 - 5.26(\text{SSA} - 0.9)]$$

The considered range for the AOD(368 nm) is 'only' [0, 1.5], thus excluding the most extreme cases that have occurred in parts of Asia.

Applying the formulas in Bodosa et al. (2002), we find that aerosol transmission has only a small dependence on SZA. The largest uncertainty is in the assumed single scattering albedo (ssa). See Table 2 below (from UVI Aerosol Extinction.xlsx). Note that the transmissions are smaller than indicated by application of the tuv model with standard values of alpha. The larger extinction that occur in practise are probably due to the increasing absorption by organic aerosols towards shorter wavelengths in the UVB region. These result in smaller single scattering albedo, as discussed by Jacobson,¹¹ and illustrated in the 2015 UNEP report.¹²

SZA (°)	T _{aer_} (SSA=0.9)	T _{aer} (SSA=0.99)
0	0.91	0.95
10	0.91	0.95
20	0.91	0.95
30	0.90	0.95
40	0.90	0.94
45	0.89	0.94
50	0.89	0.94
55	0.88	0.94
60	0.88	0.94
65	0.88	0.93
70	0.88	0.93
75	0.88	0.94
80	0.89	0.94
85	0.90	0.95

Table 2. T_{aer} as a function of SZA for AOD(368nm) = 0.3

We use the relationship above to calculate the aerosol transmission as a function of aerosol optical depth, as shown in Table 3, and Figure 6.

AOD (368 nm)	AOD (1.0 um)	AOD (0.5 um)	T _{aer} (SSA=0.9)	T _{aer} (SSA=0.99)
0.00	0.00	0.00	1.00	1.00
0.10	0.02	0.07	0.97	0.98
0.20	0.05	0.13	0.93	0.96
0.30	0.07	0.20	0.90	0.95
0.40	0.10	0.26	0.87	0.93
0.60	0.15	0.39	0.82	0.90
0.70	0.17	0.46	0.79	0.88
0.80	0.20	0.52	0.76	0.87
0.90	0.22	0.59	0.74	0.85
1.00	0.25	0.65	0.71	0.84
1.50	0.37	0.98	0.60	0.77
2.00	0.49	1.30	0.51	0.70
5.00	1.23	3.26	0.18	0.41
10.00	2.47	6.51	0.03	0.17

Table 3. Aerosol transmission at SZA=30° as a function of AOD(368). Results are shown for 2 choices of single scattering albedo. Approximate AODs are shown for other wavelength, assuming $\alpha=1.4$. For other choices of the Angstrom parameter (α), these will differ (UVI Aerosol Extinctions.xlsx)

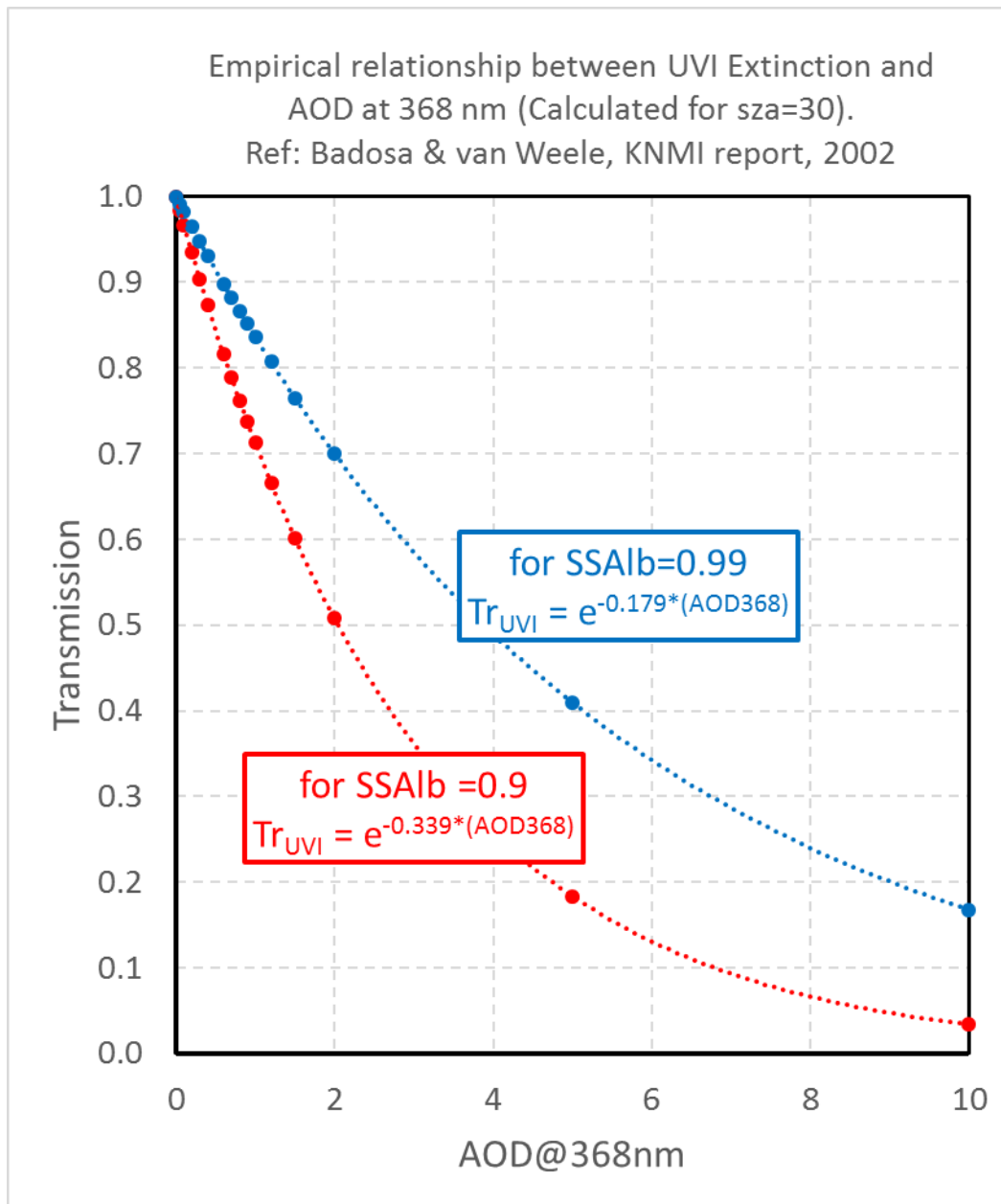


Figure 6. Aerosol transmission at as a function of AOD at 368 nm (from Table 3).

Recent studies have shown that for polluted conditions, where aerosol extinctions become important, the single scattering albedo is closer to 0.90 than to 0.99.¹³ We therefore use the relationship in the red box: $Tr_{UVI} = \exp(-0.339 \cdot AOD_{368})$. However, it should be appreciated that in reality, different aerosol mixture will have different single scattering albedos, as discussed by von Schneidemeset et al.⁶

Global Aerosol Burden

Global mean aerosol optical depth at 550 nm, along with aerosol compositions, was discussed in von Schneidemesset et al. (2015).⁶ After following up with the authors of that paper, I was able to source these mean aerosol optical depths.

Sourcing Global AOD Data

AOD data from the MODIS satellite instrument can be visualised using the Giovanni web interface: <http://giovanni.sci.gsfc.nasa.gov/giovanni/>. A sample output is shown below (Figure 7). These data can also be downloaded as files in NETCDF format.

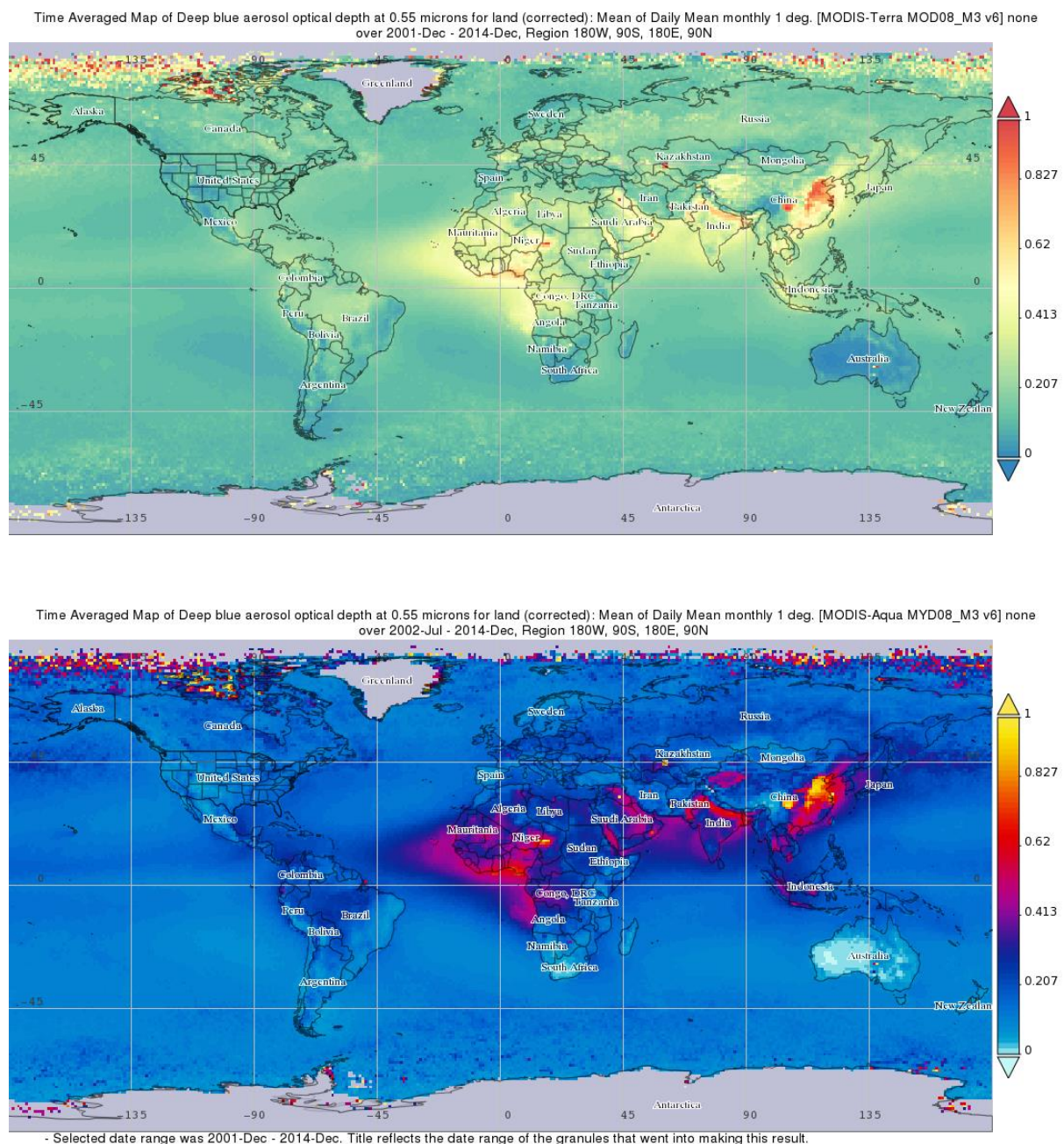


Figure 7. Long-term global mean aerosol optical depth at 550 nm, measured by Terra MODIS (upper panel), and Aqua MODIS (lower panel), as extracted from the Giovanni portal.

Climatological AODs

Dr Bjørn Hallvard Samset (b.h.samset@cicero.oslo.no) provided a 10-year MODIS Aqua climatology of AOD, which had been downloaded in NetCDF format from NSA's Giovanni site. The climatology is at a resolution of 1 degree of latitude and longitude, and covers the ten year period 2001 to 2010. File:

g4.timeAvgMap.MYD08_M3_051_Optical_Depth_Land_And_Ocean_Mean_Mean.20010101-20101231.180W_90S_180E_90N.nc Hisako Shiona at NIWA converted NETCDF file to an asci file, and I wrote an IDL program called "Map UVI App.pro" to read the values and to extract AOD values (as well as elevations at 0.5 degree resolution) at a list of sites which will be used in the GlobalUV app. Raw data are shown below in Figures 8 and 9.

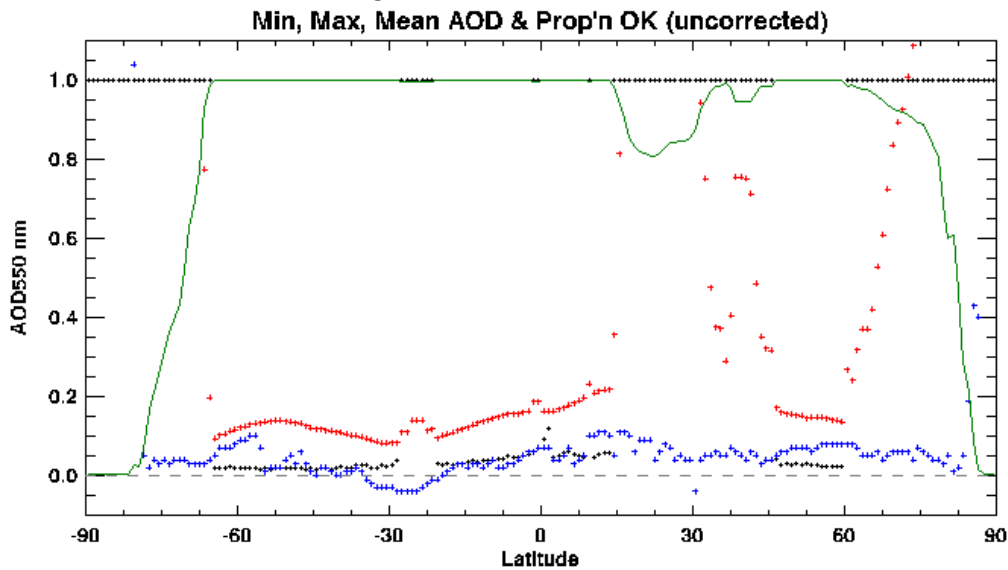


Figure 8. Min, mean, and maximum AODs for each latitude. The green line shows the fraction of values at each latitude for which data are available. See Figure 10 for other keys.

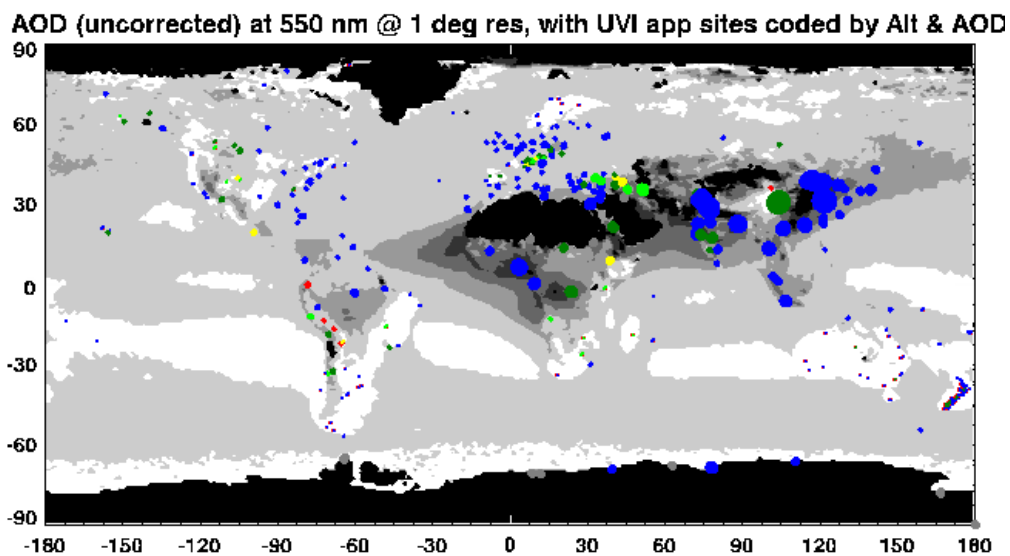


Figure 9. Uncorrected AODs at 550 nm, with site overlaid. Sites are colour coded by altitude, and size-coded by AOD. See Figure 11 for details.

Missing data, mainly at high latitudes, were interpolated as follows

1. Small negative values were replaced with mean values per latitude.
2. Values in Antarctica (latitudes >60S) were set to 0.05 to match those at nearby.
3. Values in the Arctic (latitude >60N) were set to 0.2 to match those at nearby.
4. Values in Saharan Africa were set to 0.4 to match values at similar latitudes and longitudes.
5. Forced small values to a minimum of 0.05 (to match minimum ground-measured values).

Corrected values are shown below in Figure 10 and 11.

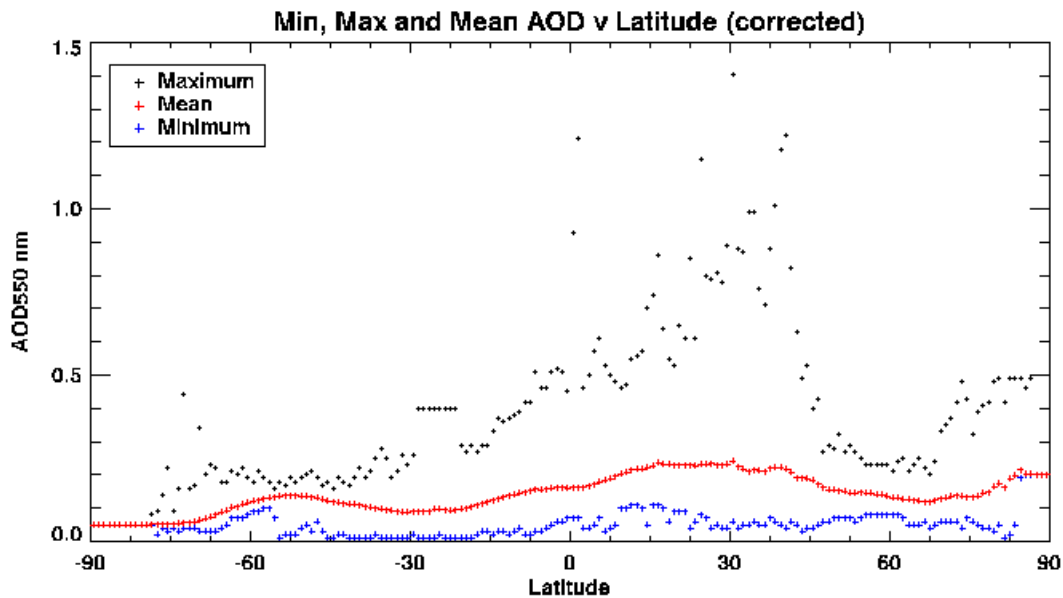


Figure 10. Min, mean, and maximum AODs for each latitude. The green line shows the fraction of values at each latitude for which data are available.

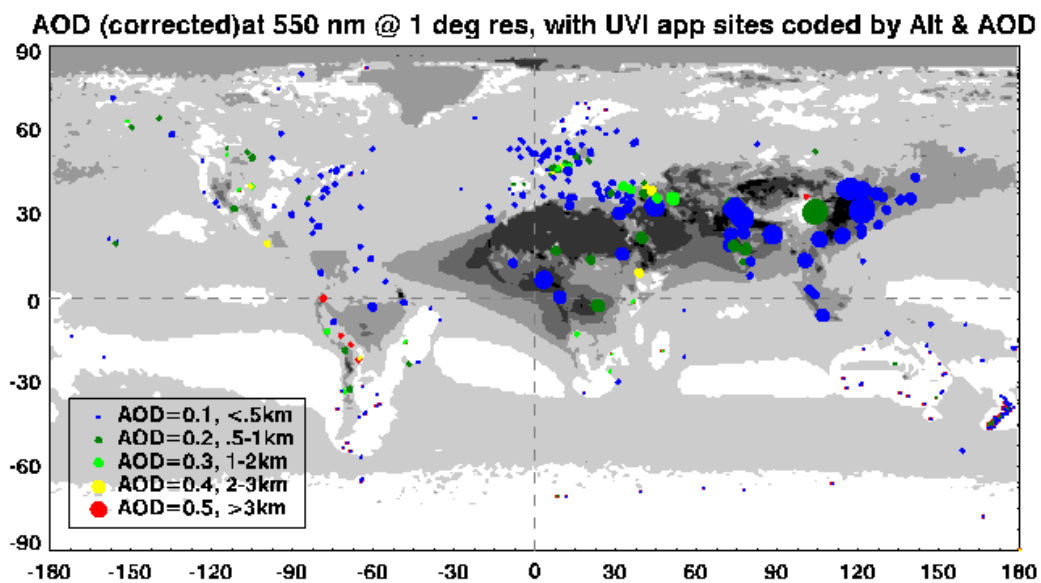


Figure 11. Uncorrected AODs at 550 nm, with site overlaid. Sites are colour coded by altitude, and size-coded by AOD.

<place-id>	<lat>	<long>	<alt (m)>	<alt_0.5deg>	<aod_368nm>	<aod_550nm>	<aod_1um>
Shanghai	31.2	121.5	10	0.01	1.45	0.82	0.35
Chengdu	30.62	104.1	500	0.54	1.36	0.77	0.33
New Delhi	28.61	77.21	216	0.22	1.21	0.69	0.29
Lahore	32	74.18	216	0.21	1.11	0.63	0.27
Tianjin	39.08	117.2	5	0	1.1	0.63	0.27
Kolkata	22.5	88.33	14	0	1.09	0.62	0.27
Hilla Babylon	32.5	44.41	40	0.03	1.04	0.59	0.25
Baghdad	33.14	44.22	30	0.04	1.01	0.57	0.25
Baoding	38.87	115.46	15	0.07	0.97	0.55	0.24
Dalian	38.54	121.36	29	0	0.96	0.54	0.23
Lagos	6.45	3.4	30	0.02	0.92	0.53	0.23
Hanoi	21	105.67	16	0.1	0.92	0.52	0.22
Hong Kong	22.28	114.17	30	0.01	0.9	0.51	0.22
Bangkok	13.5	100.29	8	0	0.81	0.46	0.2
Beijing	39.91	116.38	44	0.1	0.8	0.46	0.2
Jakarta	-6.17	106.82	30	0.05	0.74	0.42	0.18
Khartoum	15.63	32.53	405	0.4	0.74	0.42	0.18
Ahmedabad	23.05	72.67	53	0.07	0.71	0.4	0.17
Libreville	0.39	9.45	20	0.03	0.7	0.4	0.17
Kinshasha	-2.88	23.66	309	0.6	0.68	0.39	0.17
Mumbai	18.88	72.5	14	0.01	0.68	0.38	0.17
Tehran	35.7	51.42	1178	1.8	0.68	0.39	0.17
Seoul	37.35	127.03	42	0.1	0.68	0.39	0.17
Islamabad	33.72	73.07	507	0.75	0.68	0.39	0.17
Cairo	30.05	31.23	75	0.11	0.67	0.38	0.16
Pune	18.52	73.8	560	0.61	0.65	0.37	0.16
Mumbai	18.87	72.83	5	0.06	0.64	0.37	0.16
Mecca	21.42	39.82	302	0.7	0.63	0.36	0.15
Bhopal	23.28	77.47	500	0.49	0.62	0.35	0.15
Tokyo	35.68	139.68	5	0.04	0.62	0.35	0.15
Hyderabad	17.37	78.43	505	0.51	0.59	0.33	0.14
Chennai	13.08	80.3	7	0	0.57	0.32	0.14
Agades	16.97	7.98	505	0.59	0.57	0.32	0.14
Sulaimaniya	35.55	45.43	740	1.06	0.56	0.32	0.14
Tateno/Tsukuba	36.02	140.07	31	0.05	0.56	0.32	0.14
Bamoko	12.65	-8	331	0.43	0.55	0.31	0.13
Pohang	36	129.35	21	0.11	0.54	0.31	0.13
Singapore	1.3	103.8	10	0.01	0.54	0.31	0.13
Abshr	13.83	20.83	550	0.61	0.53	0.3	0.13
Kuala-Lumpur	3.11	102	150	0.24	0.53	0.3	0.13
Taipei	25.02	121.38	11	0.4	0.52	0.29	0.13
Kyoto	35.01	135.77	56	0.26	0.5	0.29	0.12

Table 4. AODs at sites where AOD368nm is greater than 0.5

Correcting for Effects of Spatial Smoothing at Specific Sites

The spatial grid of the elevation and aerosol data is 1 degree of latitude and longitude which corresponds to a footprint of dimension 100 km or more. When calculating the UVI at specific sites as specified in the sites table, the specified altitude can differ significantly from the grid value, especially for isolated peaks such as Mauna Loa Observatory (see Figure 5). Because aerosols are concentrated mainly in the lower atmosphere, their effects would be overestimated at such sites if they were interpolated from the gridded data. In that case we would have needed adjust the aerosol optical depth down for these sites, assuming an aerosol scale height of 2 km.

If $Alt_{site} > Alt_{grid}$ THEN $AOD_{368} = AOD_{368} * \exp(-(Alt_{site}-Alt_{grid})/2)$, where

Alt_{site} = altitude in km as specified in the site details

Alt_{grid} = altitude in km for the grid point corresponding to that site

However, in the GlobaUV app, this adjustment is not required, as AODs are specified in the site file (along with lat, long, alt, and alb)

Effects of Aerosols on UVI

Table 2 shows the effect of aerosol extinctions on UVI, as a function of AOD_{368nm}. For an assumed realistic single scattering albedo of 0.90, the relationship is

$$Tr_{UVI} = UVI/UVI_{clean} = \exp(-0.339 * AOD_{368}).$$

For the most polluted cities, such as in China or India, the AOD_{368nm} exceeds 1. For these locations, the clear-sky UVI is reduced by more than 30%.

For pristine locations, such as New Zealand, where the AOD is typically less than 0.05, the UVI reductions are less than 5%.

In terms of our correction factors, we have

$$f_{Aer} = [\exp(-0.339 * AOD_{368})].$$

Albedo

In the UV region, surface albedo (i.e., surface reflectance) is usually low, less than 0.05 (so only 5% of the UV irradiances is reflected). However, fresh snow has a UV surface albedo that is close to unity over snow covered surfaces. If the snow-covered surface extends several kilometres from the observation point, the resultant increase in backscattered down-welling radiation from the sky can lead to appreciable increases in UVI. For example, it has been shown the snow covered surfaces lead to increases in UVI of approximately 28%.¹⁴

Site	latitude	min (m)	max (m)
	90°N	0	0
Svalbard	78°N	300	600
Scandinavia at the polar circle	67°N	1000	1500
Iceland	65°N	700	1100
Eastern Siberia	63°N	2300	2800
southern Scandinavia	62°N	1200	2200
Alaska Panhandle	58°N	1000	1500
Kamchatka (coastal)	55°N	700	1500
Kamchatka (interior)	55°N	2000	2800
Alps (northern slopes)	48°N	2500	2800
Central Alps	47°N	2900	3200
Alps (southern slopes)	46°N	2700	2800
Pyrenees	43°N	2600	2900
Corsica	43°N	2600	2700
Caucasus	43°N	2700	3800
Pontic Mountains	42°N	3800	4300
Rocky Mountains	40°N	3700	4000
Karakoram	36°N	5400	5800
Transhimalaya	32°N	6300	6500
Himalaya	28°N	6000	6000
Pico de Orizaba	19°N	5000	5100
Rwenzori Mountains	1°N	4700	4800
Mount Kenya	0°	4600	4700
New Guinea	2°S	4600	4700
Andes in Ecuador	2°S	4800	5000
Kilimanjaro	3°S	5500	5600
Andes in Bolivia	18°S	6000	6500
Andes in Chile	30°S	5800	6500
North Island, New Zealand	37°S	2500	2700
South Island, New Zealand	43°S	1600	2700
Tierra del Fuego	54°S	800	1300
Antarctica	70°S	0	400
South Pole	90°S	0	0

Table 5. Altitude of the snow line as a function of latitude. Taken from https://en.wikipedia.org/wiki/Snow_line, accessed 4 November 2015.

In Figure 12, we show the snow line as a function of latitude, along with polynomial fits to the data.

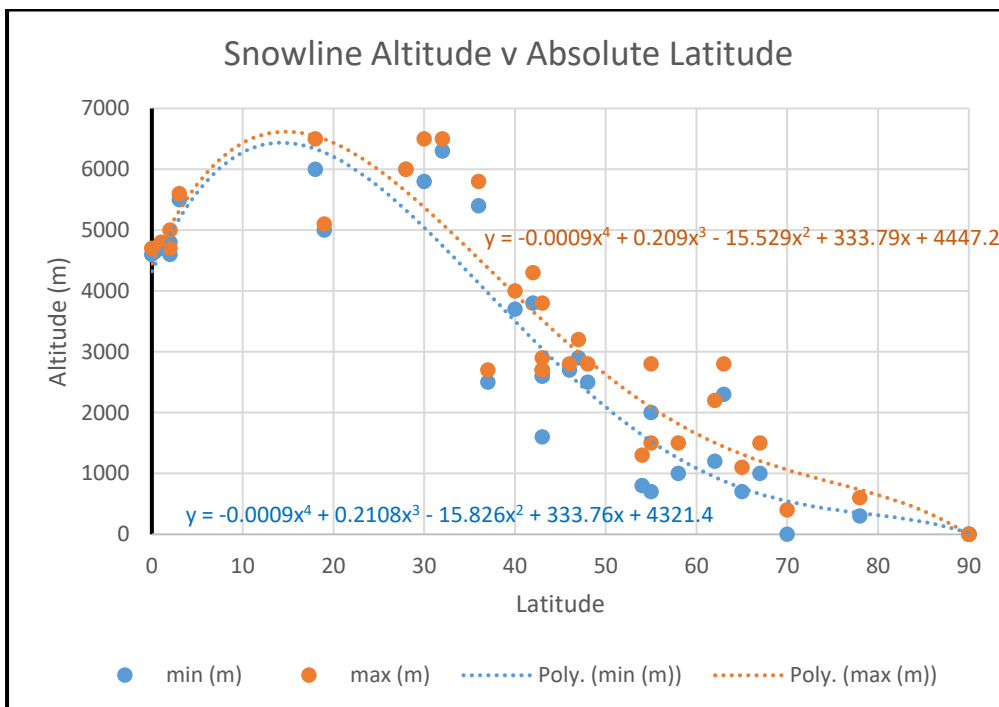
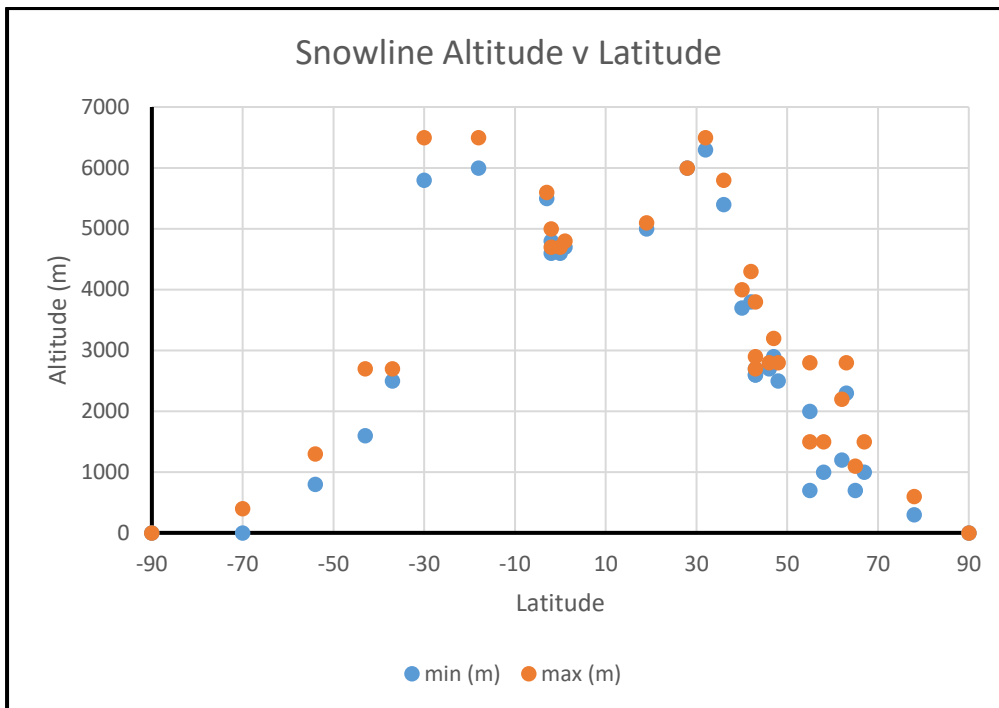


Figure 12. Upper panel: Snow line as a function of latitude. Lower panel: snow line as a function of absolute latitude, with 4th order polynomial fits.

If the altitude is greater than the upper polynomial value (brown curve), one could assume there is full snow cover. If it exceeds the lower curve, but is less than the upper curve, then assume partial snow cover. However, the uncertainties do not warrant the use of the polynomial. Instead, we just assume use a bi-linear approximation, with the snow line increasing linearly from 4.5 to 6.0 km between the equator and latitude 30, and then decreasing linearly from 6.0 to 0.0 km over the latitude range 30 to 80. For all lower altitudes, we will assume the surface albedo is 0.05. The green

points in Figure 13 shows an analytical representation of how the mean snowline varies as a function of latitude. Gridded altitudes, from a 0.5 degree grid are also shown, along with altitudes of the 250 specified sites. The largest outlier is Denali (Mt McKinley, Alaska, 6194 m). The other very high elevation site is Mt Licancabur in Bolivia (5920 m), which is included as it has been claimed¹⁵ (erroneously I think)¹⁶ the UV irradiances exceeding UVI=43 (and UVB > 11 Wm⁻²) have occurred at that site. It is close to where the peak UVI would be expected,² but the UVI and UVB values they recorded seem much too high.¹⁶

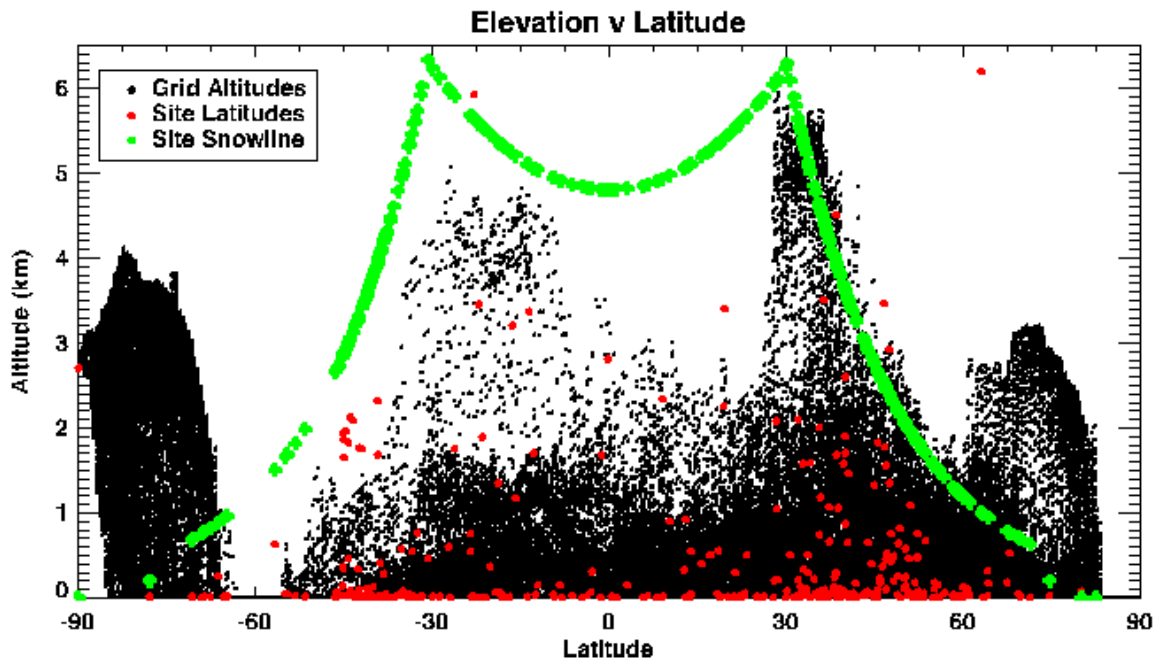


Figure 13. Latitudinal variation of climatological mean snowline, compared with all elevations represented by the 0.5° grid, and actual elevations of selected sites.

Effects of Albedo on UVI

Albedo essentially means “reflectivity”. Here we are concerned with the reflectivity in the UV region of the spectrum. In the visible region of the spectrum, most natural surfaces (e.g., grass, sand, etc.) have a relatively high reflectivity, making them visible to the eye. In fact the reflectivity varies with wavelength, making their different colours. But in the UV region, most surfaces have albedos less than 0.05, so they reflect less than 5% of the incoming UV radiation. So, if our eyes were sensitive to those wavelengths, they would “look” very dark, even in bright sunlight. The exceptions are snow and clouds, which can reflect most of the UV radiation (albedo > 0.5). Even the down-welling UV, which we are concerned with here, increases because some of the UV reflected from the surface then gets scattered back downwards by air, through Rayleigh scattering, which becomes more important at these shorter UV wavelengths. The effects of albedo changes are relatively smaller at high altitudes, where there are fewer air molecules (though the changes due to snow cover will be more likely there).

The tuv model was used to calculate the effect on UVI of changing albedo. Results are shown in Figure 14.

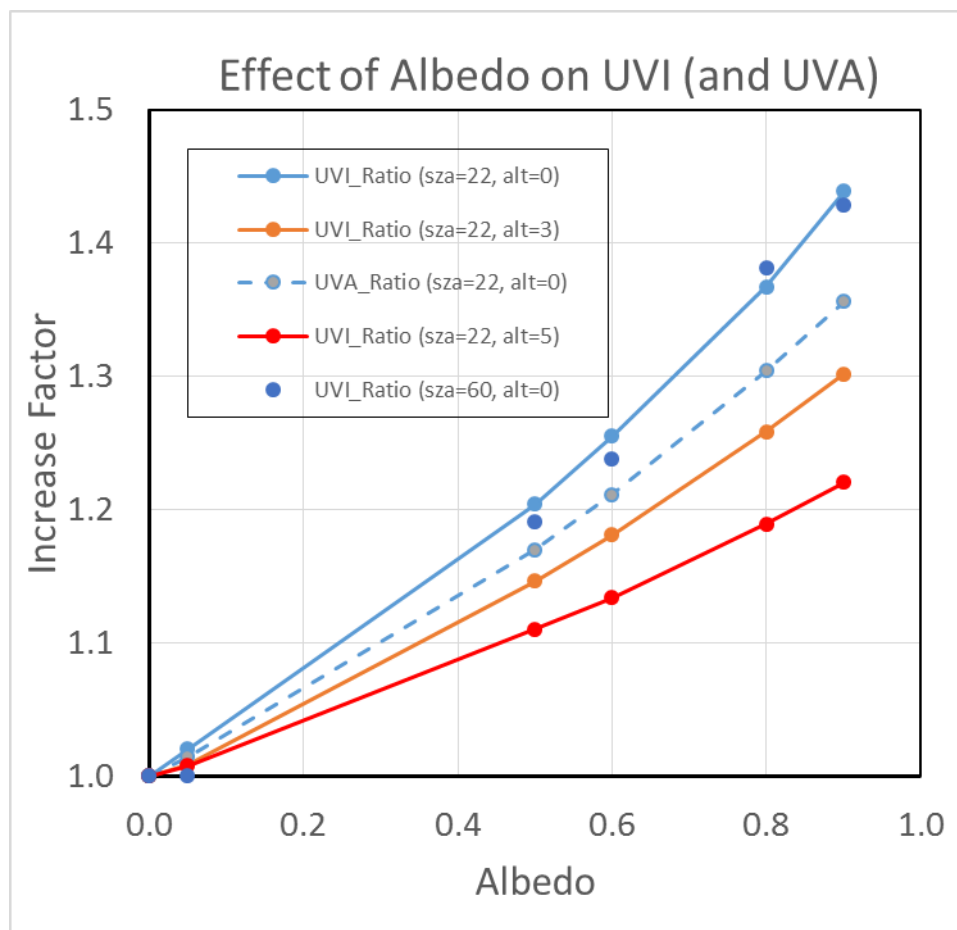


Figure 14. Calculated effect of changes in surface albedo on calculated clear sky UVI and UVA for three altitudes and two SZAs. Calculated with tuv (UVEry version) for 45.04°S (Lauder, NZ) at the summer solstice (21 Dec) at local solar noon (SZA=22°) and at SZA=60°.

Effects are a function of altitude, because at higher altitudes there is less air to backscatter the snow-reflected radiation back to the surface. For example, the increases at an altitude of 5 km (red

curve), are approximately half of those at sea level (blue curve). There is only a small dependence on SZA.

Note that for UVA irradiances (dashed curve), the effects are slightly smaller because of reduced Rayleigh backscatter at those longer wavelengths. Furthermore, in the UVA region, most surfaces have a larger albedo than in at UVI wavelengths. Consequently, the relative effects of snow cover on UVA are significantly less than for UVI.

In practice, observed increases in UV due to snow cover rarely exceed 30%, corresponding to an effective surface albedo of approximately 0.6. For surface albedos up to that value, increases are approximately linear.

The reduced effect at higher altitudes is due to the lower atmospheric pressures at those altitudes, and the increase can be approximated by the function:

$$UVI_{Alb} = UVI_{Alb=0.05} * (1 + 0.4 * alb * p/p_0), \text{ where}$$

alb is the current surface albedo

p_0 is the surface pressure (1013 hPa), and

p is the pressure at the higher altitude (e.g., 540 hPa at 5 km)

$$= UVI_{Alb=0.05} * (1 + 0.4 * \exp(-alt/7.65))$$

Note that at an altitude of 5 km, the pressure is approximately half of that at sea level, so the increase due to albedo changes is approximately halved. The relationship between altitude and pressure is shown in Table 1.

In reality, there can be huge variations in albedo due to various climatic conditions including relative humidity, and effective surface coverage.¹⁷ Consequently, attempts to model their effects will include uncertainties that are probably larger than 10%. However, even with this limitation, it is preferable to include them, as ignoring the effect would lead to systematic underestimations of UVI by 30% or more. Finally, it must be noted that there have been instances where surface albedo has been higher than 0.6. For example, albedo values greater than 0.7 and 0.9 have been observed in the Arctic and Antarctic respectively.^{17, 18} In these extreme cases, the linear approximation implicit in the above expression will lead to a slight underestimation of the UVI under such high albedo conditions.

In terms of our correction factors,

$$f_{Alb} = 1 + [0.4 * alb * \exp(-alt/7.65)], \text{ where}$$

alb = 0.05 is the default value, as used in the lookup table

= 0.7 if the altitude is above the mean latitudinal snow line

= 0.7 in the Arctic (poleward of 70N)

= 0.8 in Antarctica (poleward of 80S)

Clouds

Cloud forecasts are not specifically included in the default version because the main cloud parameter affecting the UVI is whether or not the solar disc is obscured by cloud. This parameter is extremely difficult to forecast accurately, and is better judged by the person on the spot. Typically, the cloud effects at any given site are bimodal, with a lower cloud-obscured peak at about 50% of the clear-sky peak, showing that UVI reduces by approximately 50% if the solar disc is obscured. However, there is a large spread in these reductions, as shown by Figure 15. Although the actual reduction depends on cloud optical depth, it is reasonable to assume a 50% reduction if no shadow can be discerned. Clouds in the vicinity of the sun can also lead to enhancements of UVI, by up to ~30%. However, these are only for short periods, and over time scales of a few minutes or more, the sun is obscured, and the net reduction over extended periods is always a reduction in UVI.

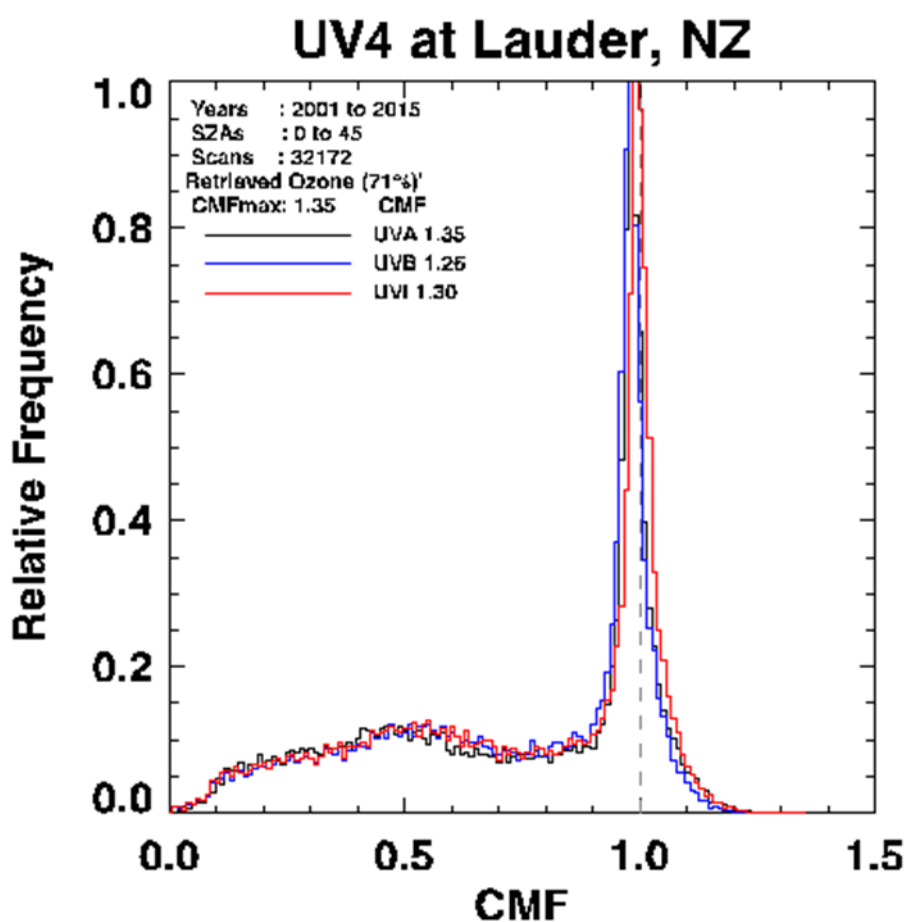


Figure 15. Bimodal distribution in UVI (and other weightings) due to cloud effects. The cloud modification factor is simply the measured UV divided by the calculated corresponding clear sky value.

If sun not obscured by cloud, $f_{\text{cloud}} = 1$, otherwise $f_{\text{cloud}} = 0.5$ (with a large uncertainty).

This cloud factor will have some dependence on other parameters. For example, when the sun is on the horizon, the Rayleigh optical depth in the UVB region is such that the solar disc is not visible. Model calculations verify that the above approximation fails at large solar zenith angles, large optical

depths, high albedo, and high altitudes. For all such conditions, the diffuse fraction can differ markedly from the example shown in Figure 15. These differences are summarised in Figure 16,

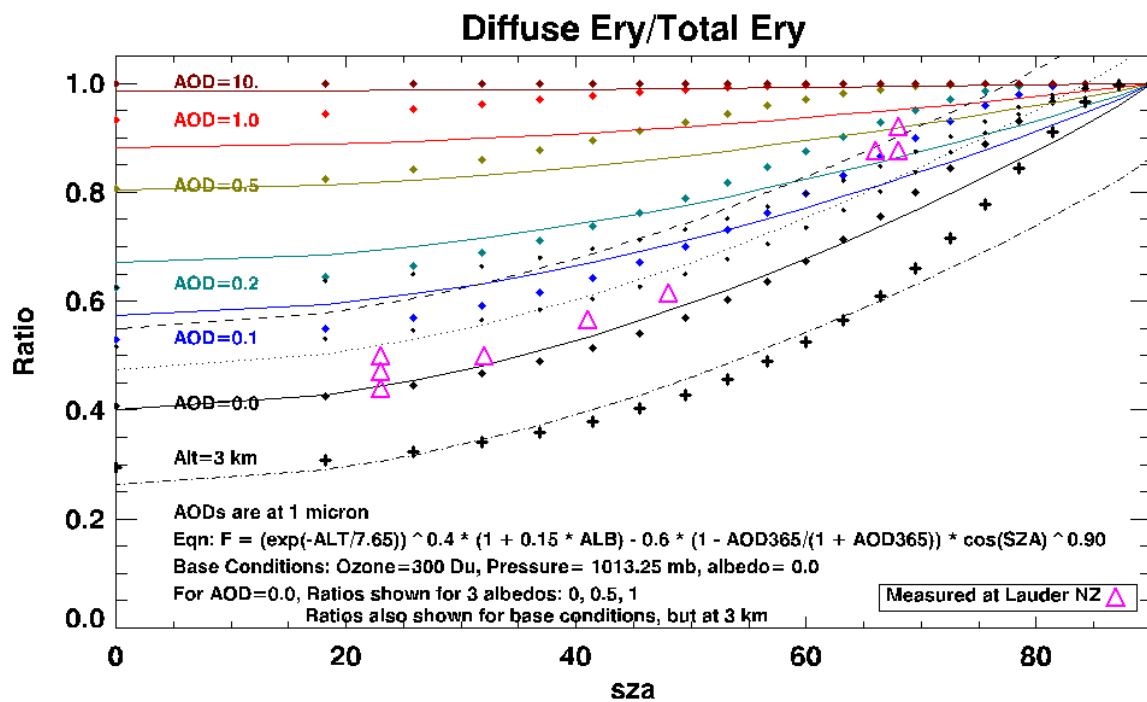


Figure 16. Diffuse fraction of UVI as a function of SZA for several choices of AOD, ozone, albedo, and altitude. Results are calculated with the tuv model, using the discrete ordinate option with 8 streams (small symbols). The large symbols are measurements, and the lines are fits using the analytic function described below.

The figure shows that the diffuse fraction:

- decreases linearly as a function of sza
- decreases with altitude - by 0.1 at 3 km compared with sea level
- increases for high surface albedo – slope is halved for albedo 1 compared with albedo 0
- increases with optical depth – slope is halved for each 0.5 increase in AOD(365nm)
- remains close to unity for all AOD(365nm) greater than 3
- has only a small ozone dependence
- value of ~0.5 deduced from the peak of bimodal distribution in Figure 15 occurs only for small SZA, low albedo, and low altitude.

The diffuse fraction can be approximated as

$$F_{\text{sunobsc}} = 1 - 0.6 * (\cos(\text{sza}))^{1.4} \text{ for clean air, low albedo, sea level}$$

$$= 1 - 0.6 * (1 - OD_{\text{aer}} / (OD_{\text{Ray}} + OD_{\text{aer}})) * (\cos(\text{sza}))^{0.9} \text{ including AOD effects}$$

$$\text{where } OD_{\text{Ray}} = 1 \text{ for UVI }^{19}$$

$$\text{and } OD_{\text{aer}} = AOD_{365\text{nm}} = AOD_{1\text{micron}} * (365/1000)^{-1.4}$$

$$= (p/p_0)^{0.4} - 0.6 * (1 - OD_{\text{aer}} / (1 + OD_{\text{aer}})) * (\cos(\text{sza}))^{0.9} \text{ also including altitude effects}$$

$$= (p/p_0)^{0.4} * (1 + 0.15 * Alb) - 0.6 * (1 - OD_{\text{aer}}) * (\cos(\text{sza}))^{0.9} \text{ also including albedo effects}$$

In terms of altitude, rather than pressure, this may be expressed as

$$F_{\text{sunobsc}} = \exp(-\text{Alt}/7.65)^{0.4} * (1 + 0.15 * \text{Alb}) - 0.6 * (1 - \text{AOD}_{365\text{nm}}) * (\cos(\text{sza})^{0.9}),$$

where the altitude (alt) is expressed in kilometres. The figure below compares ratios calculated with the tuv RT model, and fitted values using the analytic expression above.

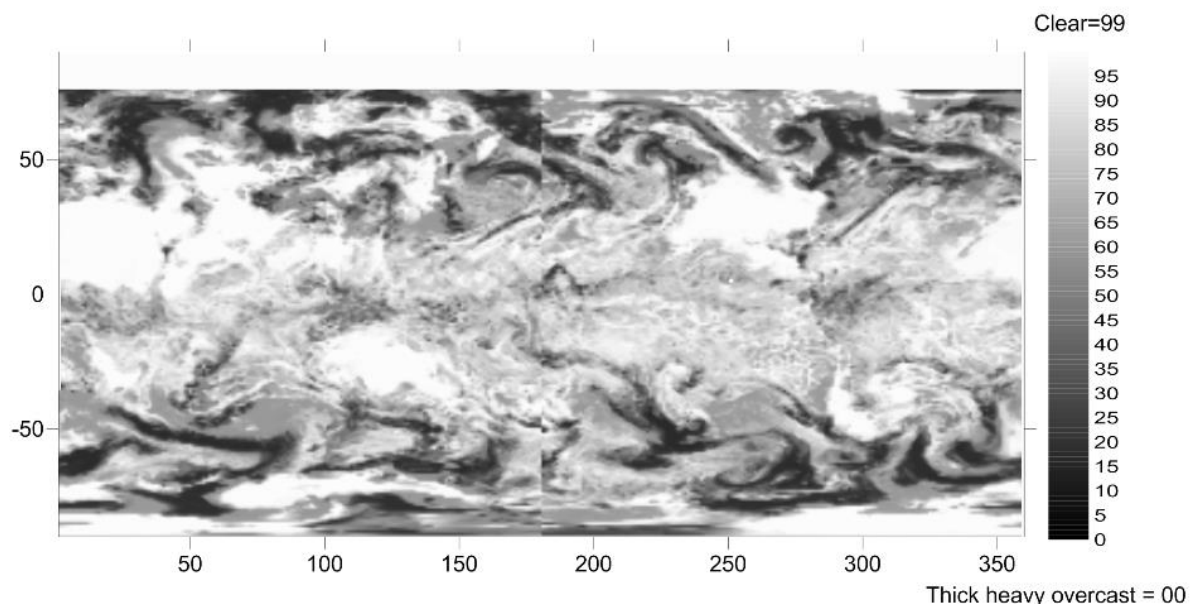
For $\text{sza} < 60$ there is good agreement between the calculated and fitted curves. Although there are significant divergences at larger sza , these are of little consequence, as UVI values for those conditions are small.

The calculated ratios above show good agreement with values derived from measurements at Lauder New Zealand, at least for $\text{SZA} < 60^\circ$, which is a pristine site for which aerosol effects are usually negligibly small. The measurement points are taken from Zeng et al.¹⁹ For larger SZA , the measured ratios are higher, but this may be due to effects of sun-visual clouds during the measurements. In the measured ratios, the largest value for $\text{SZA}=23^\circ$ was for a measurement taken in the post-Pinatubo period, when stratospheric aerosol were elevated. The largest value for $\text{SZA}=68^\circ$ was taken when there was extensive snow-cover surrounding the measurement site.¹⁹

We receive files of peak daily clear sky and cloudy sky UVI at a spatial resolution of 1 degree latitude and longitude from the Danish Meteorological Institute (DMI).

From these we calculate two files of the cloud transmission factor (CMF), one for the forecast day (CMF-day0), and one for the next day (CMF-day1), which applies for sites on west of the dateline. The same CMF is applied throughout the day.

A sample is shown below



Time Display

For the general public, the time displayed on the app should be local time, including any corrections for summer daylight saving. If that information is not available from the phone settings, it should be manually set, by specifying

Behavioural Messages

The WHO currently advises that protection is required when the UVI is 3 or more. Advice can also be given regarding the amount of time that skin can be exposed to sunlight before damage occurs (i.e., erythema). The exposure time depends on skin type, which can be self-assessed using Table 6 below. Note that these predicted exposure times are for an unshaded, horizontal surface. For skin surfaces facing the sun when it is low in the sky, exposure times can be significantly shorter than those estimated here, but these occurrences are only for relatively low UVI values.

Time for 1 MED as a function of UVI and skin type						
Skin type	I	II	III	IV	V	VI
Example Sensitivity SED/MED*	Celtic Always burns 2.5	Pale Easily burns 3.0	Caucasian May burn 4.0	Mediterranean Rarely burns 5.0	South American Rarely burns 8.0	Negro Rarely burns 15.0
UVI	Minutes of unprotected exposure before perceptible skin damage					
1	167	200	267	334	534	1001
2	83	100	133	167	267	500
3	56	67	89	111	178	334
4	42	50	67	83	133	250
5	33	40	53	67	107	200
6	28	33	44	56	89	167
7	24	29	38	48	76	143
8	21	25	33	42	67	125
9	19	22	30	37	59	111
10	17	20	27	33	53	100
11	15	18	24	30	49	91
12	14	17	22	28	44	83
13	13	15	21	26	41	77
14	12	14	19	24	38	71
15	11	13	18	22	36	67
16	10	13	17	21	33	63
17	10	12	16	20	31	59
18	9	11	15	19	30	56
19	9	11	14	18	28	53
20	8	10	13	17	27	50
21	8	10	13	16	25	48
22	8	9	12	15	24	45
23	7	9	12	15	23	44
24	7	8	11	14	22	42
25	7	8	11	13	21	40

Table 6. Calculated approximate exposure time in minutes before perceptible skin damage occurs (1 MED, minimum erythemal dose) as functions of skin type and UVI. The skin types and sensitivities to UV exposure are from ref. 13. Colours associated with the UVI values are a modified and extended version of those suggested by WHO. The shading from the lightest to the darkest corresponds to exposure times up to 10 minutes, 20 minutes, 30 minutes, 60 minutes, 120 minutes, and greater than 120 minutes respectively. From ref.³

These exposure times for skin damage may be calculated as

$$T = (f_{\text{skin}}/3.0) * (200/\text{UVI}) \text{ minutes,}$$

$$= (200 * f_{\text{skin}})/(3*\text{UVI})$$

where

f_{skin} is the corresponding skin sensitivity factor (in SED/MED) shown in the table

MED is the erythemally-weighted irradiance dose for damage to that skin type (Jm^{-2})

SED is the standard erythemally-weighted irradiance dose (1 SED = 100 Jm^{-2})

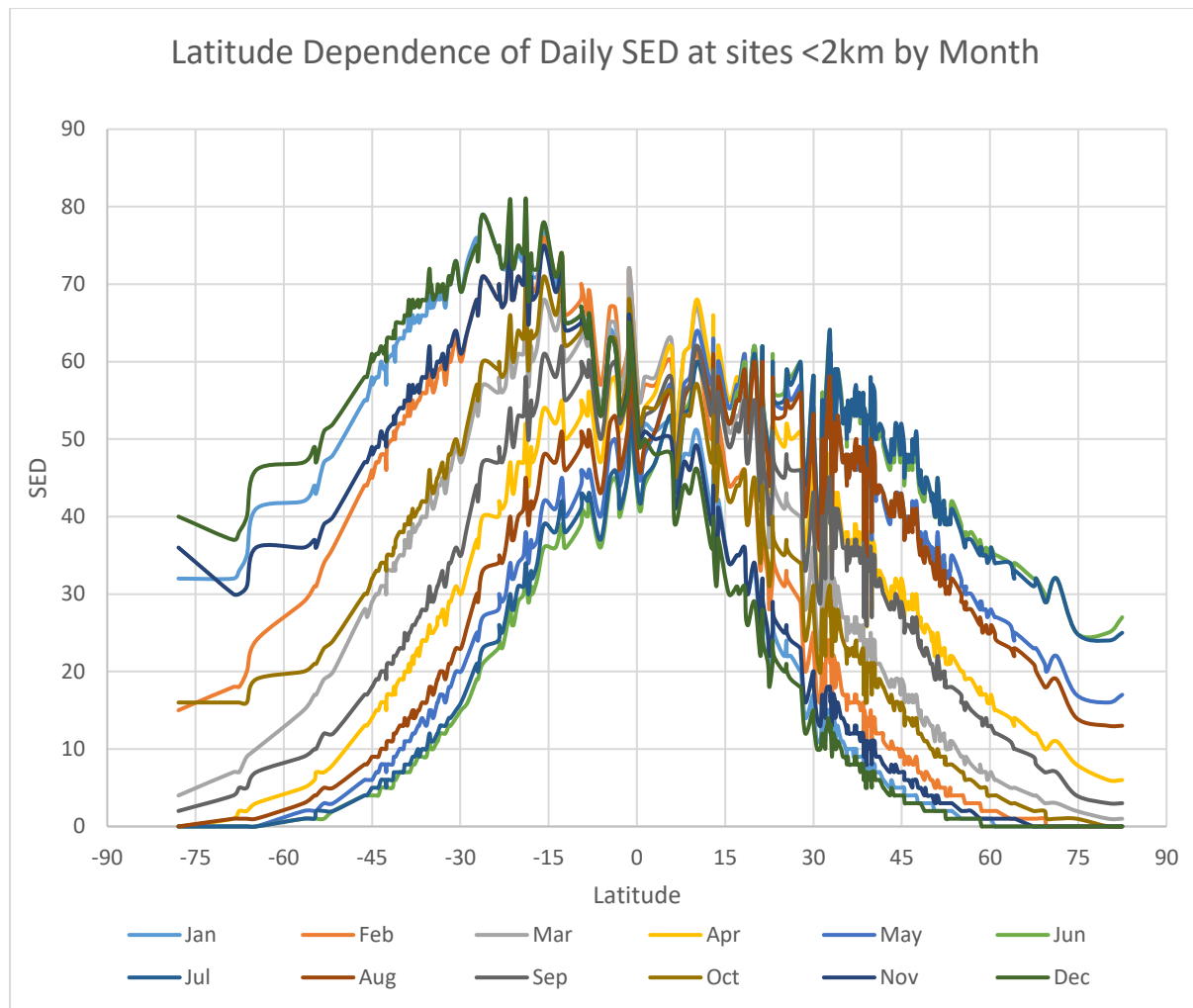
The table above is based on the upper end of Fitzpatrick classifications (see table below, reproduced from ref.²⁰). However, for the most sensitive Celtic skin type, we adjust the factor down to its mid-range values of $f_{\text{skin}} = 2.25$.

Table 1. Skin type classifications according to the Fitzpatrick scale (32) and the Australian/New Zealand Standard (58).

Skin type	Description	SED to burn	
		Fitzpatrick (1988)	Aust/NZS (2002)
I	Celtic (always burns)	2–3	<2.5
II	Pale (burns easily)	2.5–3	2.5
III	Caucasian (may burn)	3–5	3.5
IV	Mediterranean (burns rarely)	4.5–6	4.5
V	S. American (rarely burns)	6–20	–
VI	Negroid (rarely burns)	6–20	–

Validation Results from GlobalUV

Latitudinal and Seasonal dependence at sites less than 2 km altitude



The highest UV dose is around 80 SED, corresponding to 40 sunburns per day for fair skin. These highest values all occur in the SH due to lower ozone, closer Earth-Sun separation in summer, and cleaner air. Still higher values occur at the high altitude sites. For example, at MLO, the peak doses are close to 100 SED.

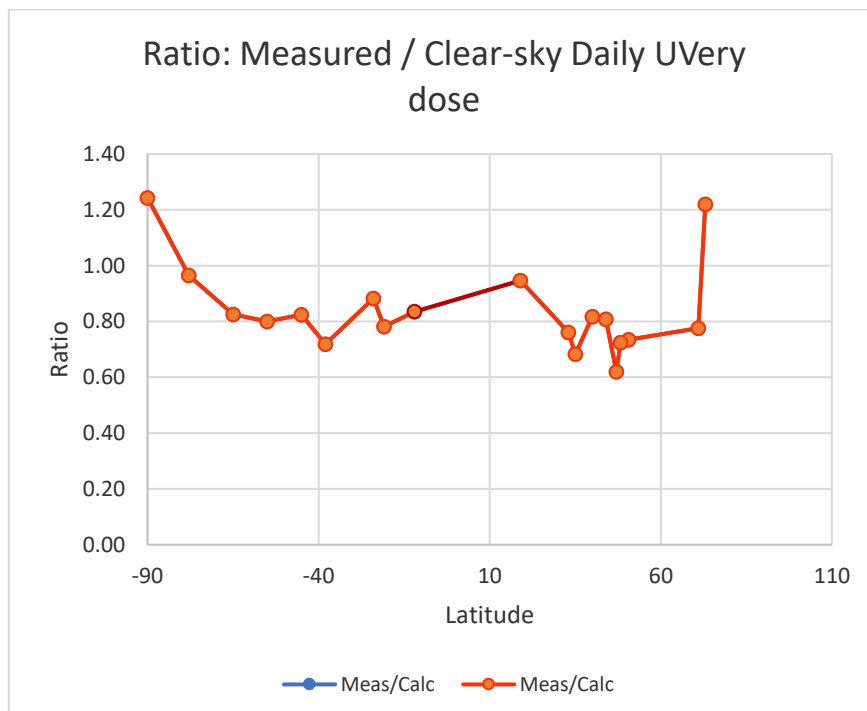
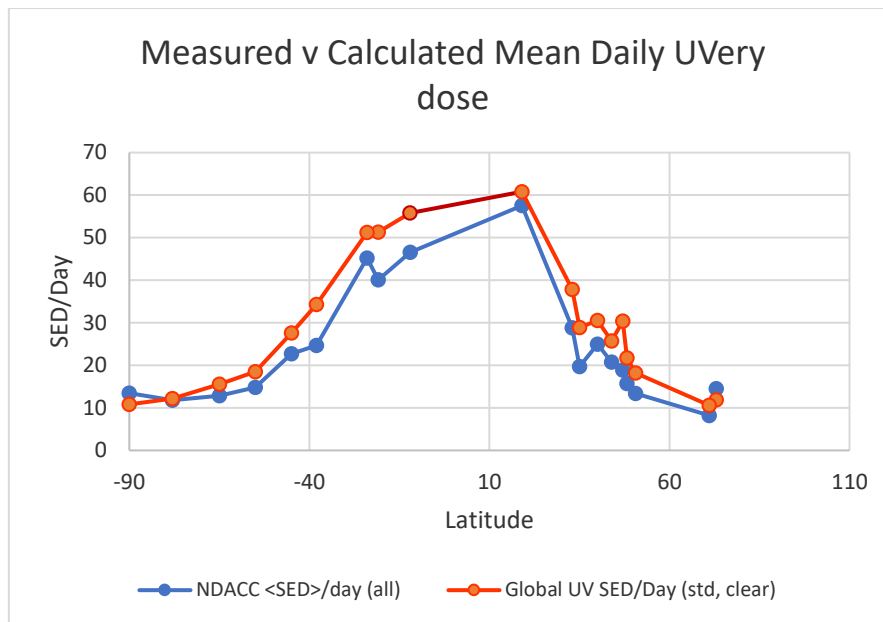
Much greater peak UV doses in the SH summer than in the NH summer due to the combined effects of (a) lower ozone, (b) higher altitude, and (c) cleaner snow with higher surface albedo. In Nov-Dec-Jan, the UV doses in Antarctica exceed 30 SED (i.e., 15 sunburns for fair skin).

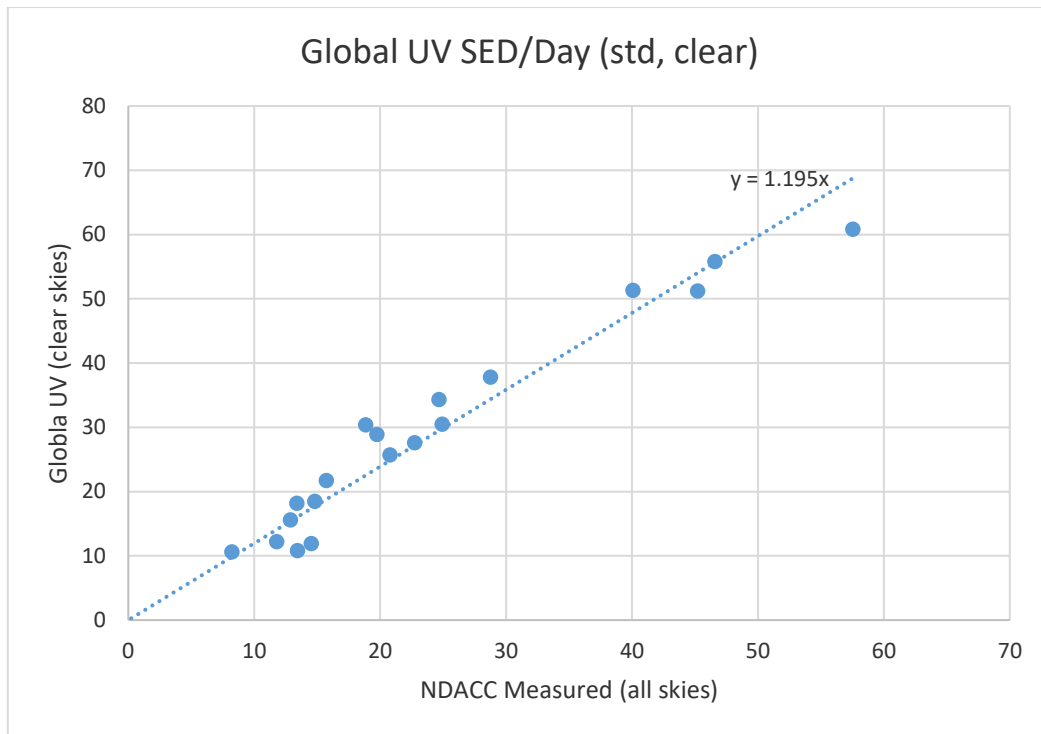
The seasonal behaviour at Lauder (45S) is as expected, with summer doses being more than a factor of ~12 greater than winter doses, consistent with summer/winter differences in peak UV and day length.

The above figure clearly shows a strong asymmetry between hemispheres, with higher UV doses in the SH summer compared with the NH summer. For example, at latitude 45°, summer values are 20% greater in the SH than in the NH. In the winter, UV doses are also larger in the SH.

Comparison with Measurements

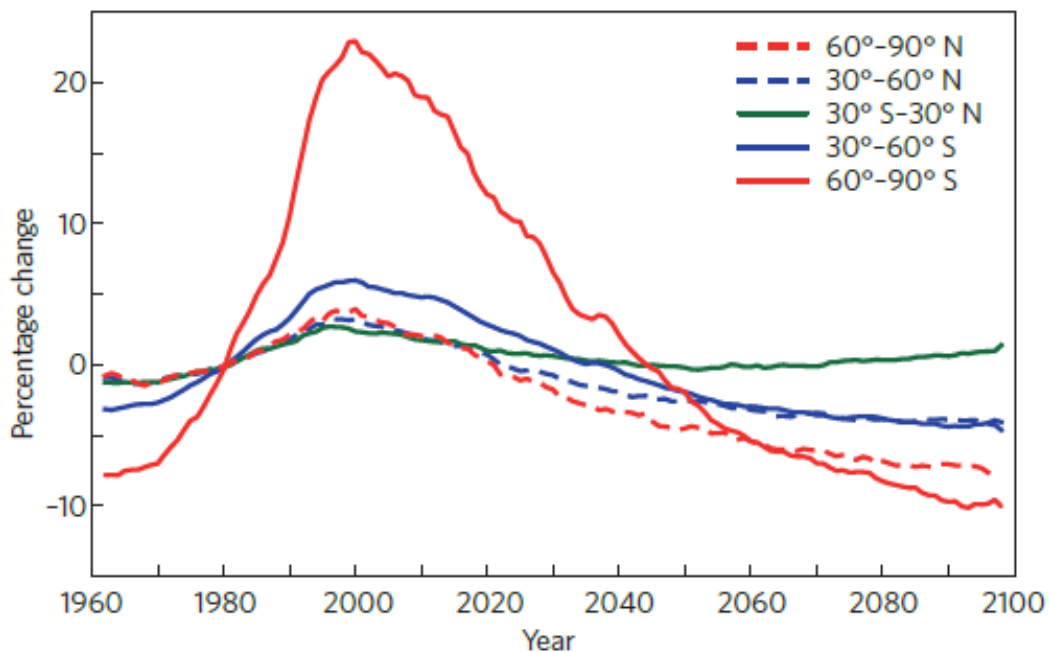
The plot below compares clear sky annual doses with measured doses at NDACC sites. Because of the inclusion of cloud effects, which typically reduce irradiances to ~0.7 of clear sky values, the measured values are expected to be lower than the app clear-sky app results by a similar factor. However, at some site, such as MLO, cloud reductions are much smaller.





Discrepancies may be expected at high latitudes – especially in the southern hemisphere - because ozone amounts over the period of NDACC measurements were lower than at the time of the 1990 ozone climatology used. Better agreement though that period may be possible using a later climatology, though as we move in the future the 1990 climatology may again be the most appropriate. Outside Antarctica, errors in UVI from this source are less than 5 percent.

The plot below shows differences in the UVI calculated with the ozone global climatology compared with measured and predicted annual ozone means for 5 latitude bands. Renormalised to differences relative to 1980.



Appendix 1.

2- Dimensional Lookup Table

The first few lines of the 2-dimensional lookup file is shown below..

File: UVI Lookup_step5.dat

Table for 1 AU

TUV 4.1 output. Version by RLM. Altitude = 0 km (Sea level)

Ozone range 100 to 600. SZA range 00 to 90

step sizes for ozone and sza 5 5

Toz SZA UVI

(DU)(Deg)

100 0 43.496

100 5 43.100

100 10 41.930

100 15 39.985

Or, if UV outputs other than just UVI are needed

File: Lookup_step5_alt0.0km.dat

Table for 1 AU

TUV 4.1 output. Version by RLM. Altitude = 0 km (Sea level)

Ozone range 000 to 600. SZA range 00 to 90

step sizes for ozone and sza 5 5

Toz SZA UVI UVB UVB* UVA

(DU)(Deg) ***** Wm-2 *****

0 0 241.090 0.112E+02 0.136E+02 0.676E+02

0 5 239.804 0.111E+02 0.135E+02 0.673E+02

0 10 235.965 0.109E+02 0.133E+02 0.663E+02

0 15 229.402 0.106E+02 0.129E+02 0.647E+02

0 20 220.661 0.102E+02 0.125E+02 0.626E+02

0 25 209.647 0.972E+01 0.119E+02 0.598E+02

0 30 196.719 0.913E+01 0.111E+02 0.566E+02

0 35 181.681 0.844E+01 0.103E+02 0.528E+02

0 40 165.013 0.767E+01 0.938E+01 0.485E+02

0 45

5-Dimensional Lookup Table

File: tuv_lookup_uvapp.dat

Note that the steps are in $\cos(\text{SZA})$, rather than SZA itself.

Z O3 AOD Albedo SZA UVERY(W/m²) UVA(?)

'TUV UVERY Lookup Table 'DS 20151117

'TUV code: tuv_ecoconnect.f

'Default TUV 4.1a model parameters:

'Altitude grid: 0-80km, z(1) = gndlvl, 1km layers

'Spectral grid: 280-400nm, 1nm spacing, 121 intervals

'Atmospheric and ozone profiles: USATM 76, 45N

'Clouds: nil

'Aerosol single scattering albedo: 0.90

'Aerosol asymmetry factor: 0.61

'Aerosol wavelength dependence, alpha factor: 1.0

'Earth-Sun distance factor: 1.0

'SO2 column amount: 0.0

'NO2 column amount: 0.0

'Radiative algorithm: 2 stream, plane parallel

'Column 1: surface pressure [mb], 6 values: 1013.25, 898.92, 795.41, 701.79, 541.37, 308.98

' for alts(km) 0., 1., 2., 3., 5., 9.

'Column 2: Ozone amount [Dobson units], 71 values: 0 to 700, 10 du spacing

'Column 3: Aerosol optical depth [at 1000nm], 6 values: 0, 0.1, 0.2, 0.5, 1.0, 10.0

'Column 4: Albedo, 3 values: 0, 0.5, 1.0

'Column 5: Solar Zenith angle [degrees]: 21 values 0.05 to 1.0 step 0.05 : $\cos(\text{sza}) = 0.05(\text{index}-1)$

'Column 6: UVERY [W/m²]

'Column 7: UVA (315-400) [W/m²]

161028 6

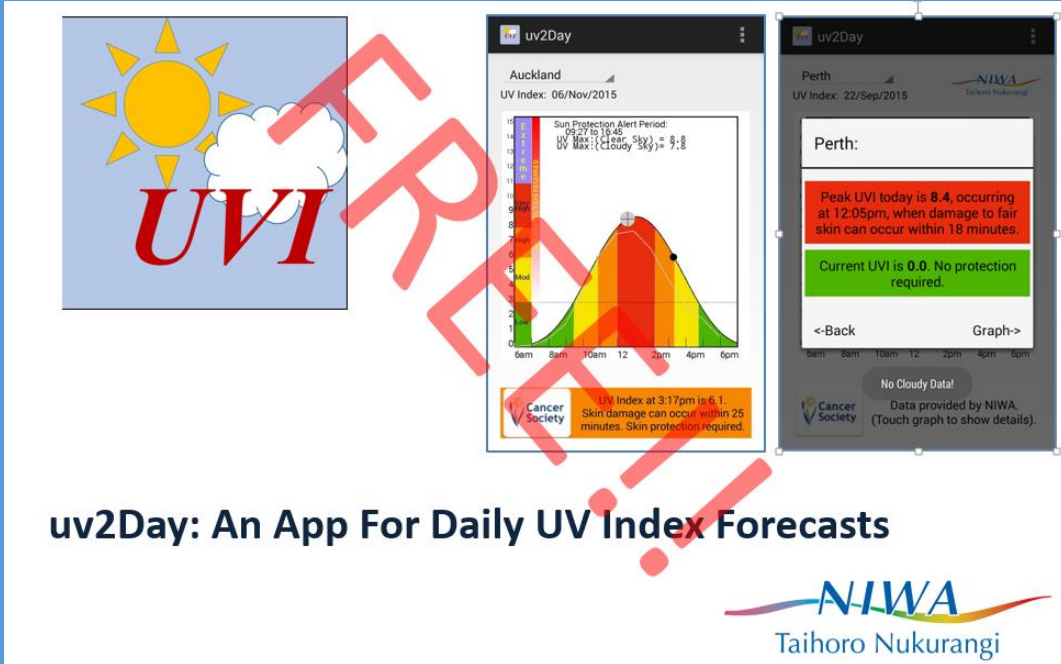
1013.25 0.00 0.0 0.0 90.00 6.720E-02 8.036E-01

1013.25 0.00 0.0 0.0 87.13 1.740E-01 2.103E+00

1013.25 0.00 0.0 0.0 84.26 3.152E-01 3.837E+00

....

Appendix 2. Uv2Day App



The image displays the Uv2Day app interface. On the left is a logo featuring a sun, a cloud, and the letters 'UVI' in red. The main part of the image shows two smartphone screens. The left screen is for Auckland on 06/Nov/2015, showing a UV index of 6.1 at 3:17pm and a sun protection alert period from 9:27 to 18:46. The right screen is for Perth on 22/Sep/2015, showing a peak UVI of 8.4 at 12:05pm and a current UVI of 0.0. Both screens include a graph of UV index over time and a 'Cancer Society' logo.

uv2Day: An App For Daily UV Index Forecasts

NIWA
Taihoro Nukurangi

The UV Index (UVI) is a measure of skin-damaging ultraviolet radiation. Unfortunately, our bodies cannot sense the damage until it is too late. This free app was developed in response to a request from the medical community to provide quantitative UVI information for New Zealanders. It is based on the UVI forecasts that NIWA has provided for many years on the internet (see <https://www.niwa.co.nz/our-services/online-services/uv-ozone>), and was written by Jeremy Burke, in consultation with Dr Richard McKenzie (NIWA). The app provides an estimate of the current UVI from sunlight, and how it is expected to vary throughout the day at your current location (or at other selectable locations). Additionally, the app provides appropriate behavioural messages. Thus it is both an educational tool, and a tool to plan your day to avoid sunburn in summer, and optimise UV exposure in winter. Forecasts for clear skies or for predicted cloud amounts are included, and the standardised UV Alert period for each day is given. The app is available for android and iPhone. Additionally, notifications are provided when standard UVI thresholds (e.g., UVI = 3, 6, 8, etc) are exceeded. The app is limited to New Zealand, Australia, the Pacific, and Antarctica; but a version with global coverage is under development.

Although small amounts of UV radiation are beneficial to health, overexposure can lead to skin cancer. New Zealand and Australia have the highest rates of skin cancer in the world, and the Cancer Societies of both countries recommend that you take protection whenever the UVI is greater than 3. The main determinant of UVI is the sun's elevation angle, so UVI values are greatest in the summer, especially near solar noon (typically around 1:30 pm in the NZ summer). In winter, peak UVI values are generally less than 2, but in summer they can exceed 12. These peak values are about twice as high as in the UK, but the highest values in the world occur in the high altitude Altiplano region of Peru, where they can exceed UVI=25. In New Zealand and Australia, UVI values are considered "extreme" when they exceed 10. For that UVI value, skin damage in fair skinned people can occur in about 15 minutes, so it is important to take steps to protect yourself by avoiding direct sunlight, or by liberally applying a sunscreen with a high SPF factor to exposed skin.

Appendix 3. GlobalUV App



This App provides estimates of the current UVI and how it is expected to vary throughout the day at your current location or at any other locations throughout the globe. It also provides behavioural advice on how long you can remain in sunlight before damage occurs for your selected skin type. It is an educational tool that helps you plan your day to optimise your UV exposure.

The app is an extension of the uv2Day app (developed in collaboration with NIWA) which applies only to the Pacific region, where aerosol extinctions are small. Unlike that app, GlobalUV uses forecasts of ozone and cloud effects to calculate UVI on the fly. At a small cost in speed, there is a huge benefit in versatility. In addition, it provides information about position, altitude, sun elevation angle, ozone amounts, aerosol extinctions, and effects of clouds and surface reflectance (e.g., due to snow cover). Additionally it shows the current global pattern of UVI. Finally, it can display clear-sky UVI values for other seasons at any location. Currently, it is available only for android phones.

Further Details

This app provides information about the current UVI and how it will vary throughout the day at any location. Sites can be selected by three methods: (1) GPS, (2) Drop-down menu of over 300 preloaded sites, (3) selection by touching the global map, using sliders to fine tune. Your own favourite locations can be specified and stored.

The app uses (a) daily ozone forecast maps provided by NOAA, (b) solar zenith angles calculated from location and time, (c) a look-up table to calculate the clear sky UVI as a function of ozone and solar zenith angle (SZA), (d) a digital elevation map to allow altitude corrections at other locations, (e) climatology of aerosol optical depth, (f) estimates of cloud effects at noon, and a (g) climatology map of monthly mean ozone as a function of latitude for estimating UV at other times.

The clear-sky UVI is first calculated for sea-level, assuming an Earth-Sun separation of 1 AU. Corrections are then applied to account for seasonal differences in Sun-Earth separation, altitude (including corrections to albedo due to estimated snow cover), and the climatological mean aerosol optical depth, and cloud effects for each location.

Initial outputs (portrait mode) are the calculated clear sky and UVI at the current time, and the time and value of peak UVI expected that day, along with behavioural messages that depend on the skin type entered. A world map shows the selected location and the current pattern of UVI for UVI > 3.

The second screen (landscape mode) goes into more detail, show plots of the progression in UVI throughout the day, with accompanying behavioural messages. The app displays parameters relevant to the calculation of UVI, and allows the capability to alter some of them to allow for local conditions, such as snow cover, heavier than usual pollution, or whether the sun is obscured by clouds.

The app includes a capability of estimating UVI at any location for other seasons. This is achieved by making use of a monthly climatology of ozone rather than the forecast values for the present day. This capability allows users to plan timing of visits to other destinations, or events at other locations.

The UVI can be shown in Solar Time (longitude), Phone Time (at the current location), or GMT.

Acknowledgements: The app was developed by JGR Burke (jgrburke@gmail.com) in consultation with Richard McKenzie, NIWA, Lauder, New Zealand. Further assistance was provided by Craig Long (NOAA, USA), Helge Jonch-Sorensen (DMI, Denmark), and Richard Turner and Ben Liley (NIWA, NZ).

Appendix 4. File Locations

(to be copied from *.txt – if I ever find it)

References

- 1 WHO, *Global solar UV Index: A practical guide*, World Health Organisation (WHO), World Meteorological Organisation (WMO), United Nations Environment Program (UNEP), and International Commission on Non-Ionising Radiation Protection (ICNRP), Geneva, 2002.
- 2 J. B. Liley and R. L. McKenzie, Where on Earth has the highest UV?, in *UV Radiation and its Effects: an update*, Vol. 68, RSNZ Miscellaneous Series, Dunedin, 2006, pp. 36-37 (https://www.niwa.co.nz/sites/default/files/import/attachments/Liley_2.pdf).
- 3 F. Zaratti, R. D. Piacentini, H. A. Guillén, S. H. Cabrera, J. B. Liley and R. L. McKenzie, Proposal for a modification of the UVI risk scale, *Photochemical & Photobiological Sciences*, 2014, **13**, 980-985.
- 4 A. F. McKinlay and B. L. Diffey, A reference action spectrum for ultra-violet induced erythema in human skin, in *Human Exposure to Ultraviolet Radiation: Risks and Regulations* eds.: W. F. Passchier and B. F. M. Bosnjakovic, Elsevier, Amsterdam, 1987, pp. 83-87.
- 5 R. L. McKenzie, P. V. Johnston, D. Smale, B. Bodhaine and S. Madronich, Altitude effects on UV spectral irradiance deduced from measurements at Lauder, New Zealand and at Mauna Loa Observatory, Hawaii, *J. Geophys. Res.*, 2001, **106**, 22845-22860.
- 6 E. von Schneidemesser, P. S. Monks, J. D. Allan, L. Bruhwiler, P. Forster, D. Fowler, A. Lauer, W. T. Morgan, P. Paasonen, M. Righi, K. Sindelarova and M. A. Sutton, Chemistry and the Linkages between Air Quality and Climate Change, *Chem. Rev.*, 2015, **115**, 3856–3897.
- 7 Z. Li, X. Gu, L. Wang, D. Li, Y. Xie, K. Li, O. Dubovik, G. Schuster, P. Goloub, Y. Zhang, L. Li, Y. Ma and H. Xu, Aerosol physical and chemical properties retrieved from ground-based remote sensing measurements during heavy haze days in Beijing winter, *Atmos. Chem. Phys.*, 2013, **13**, 10171–10183.
- 8 R. L. McKenzie, G. E. Bodeker, G. Scott and J. Slusser, Geographical differences in erythemally-weighted UV measured at mid-latitude USDA sites, *Photochemical & Photobiological Sciences*, 2006, **5**, 343-352.
- 9 J. Badosa and M. van Weele, Effects of aerosols on uv-index, KNMI Report No., De Bilt, p. 48. Available from:
- 10 M. Allaart, M. vanWeele, P. Fortuin and H. Kelder, An empirical model to predict the UV-index based on solar zenith angles and total ozone, *Meteorol. Appl.*, 2004, **11**, 59–65
- 11 M. Z. Jacobson, Isolating nitrated and aromatic aerosols and nitrated aromatic gases as sources of ultraviolet light absorption, *Journal of Geophysical Research*, 1999, **104**, 3527-3542.
- 12 A. F. Bais, R. L. McKenzie, G. Bernhard, P. J. Aucamp, M. Ilyas, S. Madronich and K. Tourpali, Ozone depletion and climate change: Impacts on UV radiation, *Photochemical & Photobiological Sciences*, 2014, **2015s**.
- 13 R. L. McKenzie, P. J. Aucamp, A. F. Bais, L. O. Björn, M. Ilyas and S. Madronich, Ozone depletion and climate change: impacts on UV radiation, *Photochemical & Photobiological Sciences*, 2011, **10**, 182-198.
- 14 R. L. McKenzie, K. J. Paulin and S. Madronich, Effects of snow cover on UV radiation and surface albedo: a case study, *Journal of Geophysical Research*, 1998, **103**, 28785-28792.
- 15 N. A. Cabrol, U. Feister, D.-P. Häder, H. Piazena, E. A. Grin and A. Klein, Record solar UV irradiance in the tropical Andes, *Frontiers of Environmental Science*, 2014, **2**, 1.
- 16 R. McKenzie, G. Bernhard, S. Madronich and F. Zaratti, Comment on “Record solar UV irradiance in the tropical Andes, by Cabrol et al.”, *Frontiers in Environmental Science*, 2015, **3:26**.
- 17 O. Meinander, S. Wuttke, G. Seckmeyer, S. Kazadzis, S. Lindfors and E. Kyrö, Solar zenith angle asymmetry cases in polar snow UV albedo, *Geophysica*, 2009, **45**, 183-198.

- 18 S. Wuttke, G. Seckmeyer and G. König-Langlo, Measurements of spectral snow albedo at Neumayer, Antarctica, *Annales Geophysicae*, 2006, **24**, 7-21.
- 19 J. Zeng, R. McKenzie, K. Stamnes, M. Wineland and J. Rosen, Measured UV spectra compared with discrete ordinate method simulations, *Journal of Geophysical Research*, 1994, **99**, 23019-23030.
- 20 R. L. McKenzie, J. B. Liley and L. O. Björn, UV Radiation: Balancing Risks and Benefits, *Photochemistry and Photobiology*, 2009, **85**, 88-98.